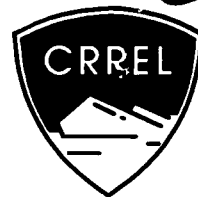


AD-A280 752



①

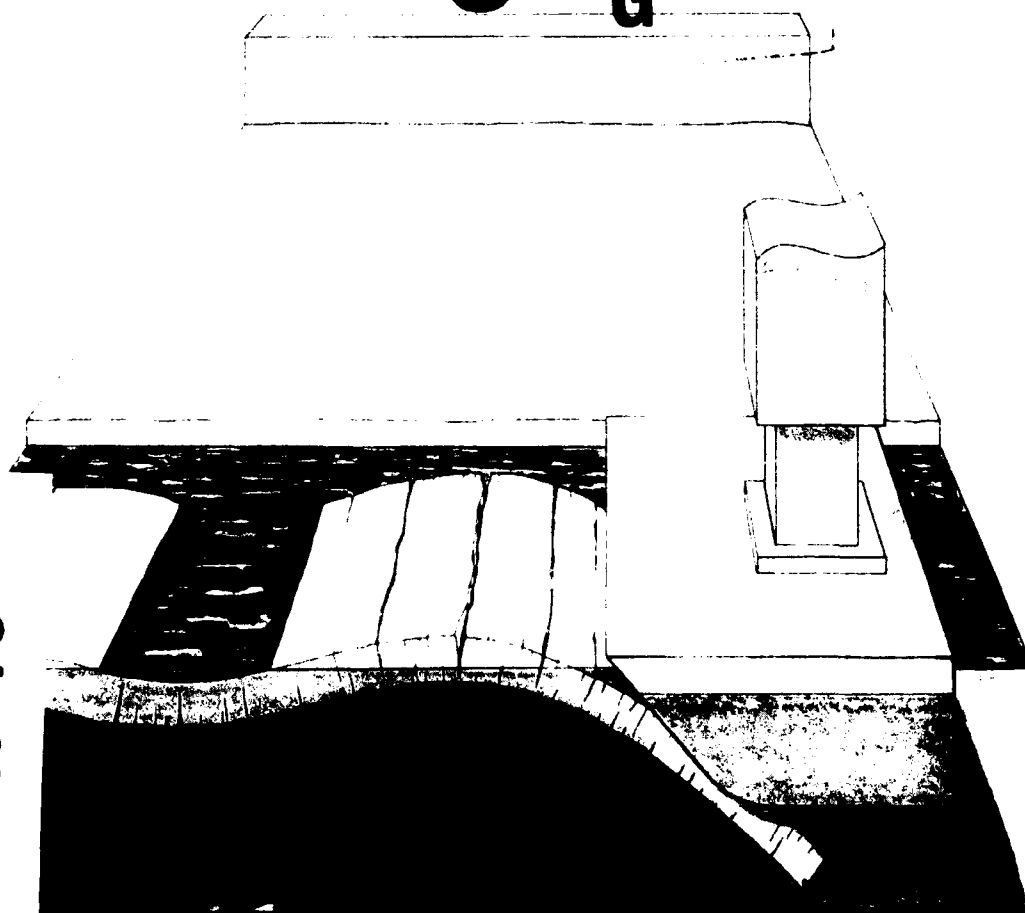
Experimental and Numerical Analysis of Floating Ice Beam Impact Forces Against a Sloped Structure

Barry A. Coutermarsh

March 1994

DTIC
ELECTE
JUN 28 1994
S G D

94-19696



94 6 28 0 5 5

**Best
Available
Copy**

Abstract

Floating ice impact forces are of concern where structures are built in ice-susceptible waters. Bridge piers, ice control structures or icebreakers are a few examples where the ability to predict the expected ice impact force would be of great help in the design process. Experiments were performed to determine the response of a floating ice beam to a vertically applied force. The data were used to calibrate a numerical finite element model of the floating ice. The ice was characterized as a linear elastic material in the numerical analysis, and the calibration data were used to assess this assumption as well as to develop a fluid influence coefficient matrix to simulate the dynamic influence of the fluid beneath the ice beam. Finally, a scale model study was performed to determine actual impact forces generated by a floating ice beam against a 45° sloped structure. The numerical model developed was then compared to the actual data. The numerical model does well at predicting impact forces for all the beams at low velocity and the force from the thicker ice beams at all velocities. Both the numerical and experimental forces show the same trends and appear to level off and approach a constant value with increasing beam length. The discrepancies between numerical predictions and experimental results are thought to be caused by damage in the experimental ice beams which is not accounted for in the numerical model.

For conversion of SI metric units to U.S./British customary units of measurement consult ASTM Standard E380-89a, *Standard Practice for Use of the International System of Units*, published by the American Society for Testing and Materials, 1916 Race St., Philadelphia, Pa. 19103.



**U.S. Army Corps
of Engineers**
Cold Regions Research &
Engineering Laboratory

Experimental and Numerical Analysis of Floating Ice Beam Impact Forces Against a Sloped Structure

Barry A. Coutermarsh

March 1994

Accession For	
NTIS	CRA&I <input checked="" type="checkbox"/>
DTIC	TAB <input type="checkbox"/>
Unannounced <input type="checkbox"/>	
Justification	
By	
Distribution /	
Availability Codes	
Dist	Avail and/or Special
A-1	

DTIC QUALITY INSPECTED

PREFACE

This report was prepared by Barry A. Coutermarsh, Research Civil Engineer, Applied Research Branch, Experimental Engineering Division, U.S. Army Cold Regions Research and Engineering Laboratory, as one of the requirements for his M.S. degree from the Thayer School of Engineering, Dartmouth College, Hanover, New Hampshire.

The author thanks the members of his thesis committee (Dr. Francis E. Kennedy, Dr. Devinder S. Sodhi and Dr. Ian Baker) for taking the time to serve in this capacity and for their help and advice in the thesis. He also thanks the many people at CRREL—of special note are Gary Phetteplace and Paul Richmond, who provided support with funds and encouragement, and Randy McGilvary for his belief in and enthusiasm for the work that comprises this report. His patient explanations of his fluid influence coefficient work have been instructive and invaluable. The author also thanks his parents for their unwavering belief in the value of education and their solid support in education throughout his life.

CONTENTS

Preface	ii
Introduction	1
Background	1
Theory	2
Model similitude	3
Experimental procedure	3
Preliminary tests	5
Numerical procedure	5
Beam response	7
Experimental results	9
Results and discussion	16
Prototype forces	22
Conclusions	23
Literature cited	24
Appendix A: Preliminary results and analysis	25
Appendix B: Test data	31
Appendix C: Procedure flow chart	39
Abstract	40

ILLUSTRATIONS

Figure

1. Profile of U.S. Army floating ribbon bridge	2
2. Test setup	4
3. The finite element model of the bridge and ice beam	6
4. Plots of static foundation reaction force and foundation modulus with respect to displacement, for an ice node	6
5. Schematic diagram of a floating ice beam instrumented with LVDTs	7
6. Typical results from an 8-m-long beam response experiment.....	8
7. Comparison of numerical and experimental beam displacement histories for a 4-m-long beam	9
8. Comparison of numerical and experimental beam displacement histories for an 8-m-long beam	10
9. Comparison of numerical and experimental beam displacement histories for an 15.25-m-long beam	11
10. Typical plot of forces vs. time data from the experiments	12
11. Average peak impact force vs. beam length and beam thickness, for the replicated experiments, at 0.1524 m/s	13
12. Average peak impact force vs. beam length and beam thickness, for the replicated experiments, at 0.6096 m/s	13
13. Average peak impact force vs. beam length and beam thickness, for the replicated experiments, at 1.0668 m/s	14

14. Average peak impact force vs. beam length and beam thickness, for the replicated experiments, at 1.524 m/s	14
15. Maximum values of F_x vs. F_z , showing a constant ratio of F_x/F_z to be approximately 1.34	15
16. A typical numerical force vs. time plot from an impact of a 1.219-m-long beam at 0.61 m/s	17
17. Comparisons of average experimental peak impact force and numerical peak impact force vs. ice beam length, at constant velocities, for a given thickness ice beam	17
18. Comparisons of average experimental peak impact force and numerical peak impact force vs. impact velocity, at constant beam lengths, for a given thickness ice beam	18
19. During impact, only the initial portion of an ice beam will contribute to the impact force as illustrated above	19
20. Comparisons of nondimensional experimental and numerical impact force vs. beam length divided by characteristic length (L/L_c), at constant beam thickness, for a given impact velocity	20
21. Nondimensional experimental and numerical force vs. nondimensional velocity	21
22. Plots of force vs. velocity, at constant beam lengths, from the numerical simulation	22

TABLES

Table

1. Fluid drag forces associated with the sudden acceleration of a flat plate for each size ice beam calculated at the highest and lowest experimental velocities	16
2. Beam thickness and associated characteristic length for the test beams	19

Experimental and Numerical Analysis of Floating Ice Beam Impact Forces Against A Sloped Structure

BARRY A. COUTERMARSH

INTRODUCTION

The force generated by a floating ice floe impacting against a structure is of interest in many engineering situations. Icebreakers, bridge piers in cold regions, and ice control and offshore structures are just a few of the structures that must withstand ice impacts. It is difficult, if not impossible, to analytically determine these forces because of the complex nature of the ice-structure interaction involving the supporting fluid, as well as the difficulty in characterizing the material response of the ice.

The initial impetus for this work was to determine the maximum force that could occur during an ice impact against the U.S. Army floating tactical "Ribbon Bridge." The bridge comes in sections that are deployed individually and then connected in the water to form a continuous bridge. Each section has two rectangular roadway pontoons and two bow pontoons with 45° sloped faces as shown in Figure 1. During its normal use in a river where floating ice might be present, the sloped faces of the bow pontoons would receive any impact.

This report describes a model study of ice impacting a 45° sloped surface. The forces generated by the impacts are analyzed using a general finite element technique with the ice characterized as a linear elastic material. The fluid/ice interaction is handled by a linear fluid inertial coupling.

The study was performed in essentially three parts. Experiments were performed to measure the response of a floating ice beam to a vertically applied force at one end of the beam. The data from these experiments were used to calibrate a numerical finite element model of the floating ice. It was used to help assess the assumption of a linear elastic material designation for the ice and to develop a fluid influence coefficient matrix that simulated the dynamic influence of the fluid beneath the floating ice beam. This step is described in the beam response section below. In the next step, a model study was performed to gather data on the actual forces generated by a floating ice beam. The impact data were then analyzed using

a finite element numerical model. These last two steps form the main body of the work and are described in detail below.

BACKGROUND

The force generated by an ice floe impacting against the ribbon bridge is difficult to determine analytically due to the unconstrained motion of both the floe and bridge.

The ribbon bridge is a series of articulated sections consisting of four floating pontoons attached by hinges and latches (Fig. 1). The bow pontoons offer a 45° sloped surface for an ice floe to impact against. This surface is free to respond to the floe's kinetic energy in a number of ways:

1. The surface itself can be indented or torn.
2. The bow pontoon can displace due to the free movement in the hinges and latches holding the pontoons together as well as through the slack in the connectors between bridge sections.
3. Entire bridge sections can translate due to the slack in the anchoring system securing the bridge in the river.
4. The pontoon can displace due to the hydrodynamic response of the floating bridge to balance the impact force.

In addition to the bridge's response, the impact energy can be dissipated in the ice through:

1. Crushing and fracturing of the ice during impact.
2. The irreversible hydrodynamic response of the fluid foundation.
3. Horizontal rotation of the floe.
4. The internal strain energy response of the ice.

Only the portion of the impact energy that is actually transferred to the bridge is capable of damaging the bridge, either through indenting or puncturing of the pontoon or failure of the connectors. The numerous ways that the floe's energy can be dissipated make it difficult to analytically quantify the amount that would be transmitted to the bridge versus that which goes into the other mechanisms mentioned above. It should also be pointed out that since material failure is of concern, it is

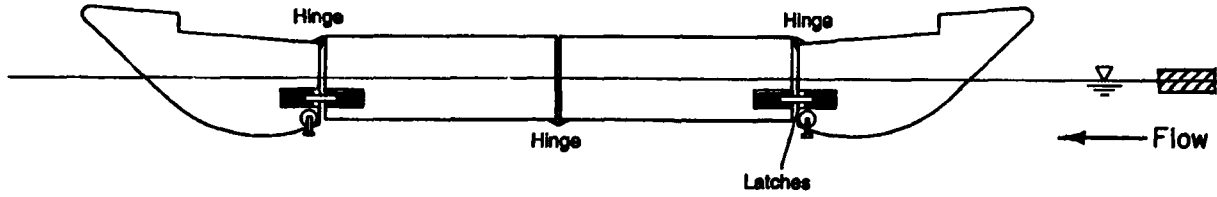


Figure 1. Profile of U. S. Army floating ribbon bridge.

necessary to determine the maximum impact force as opposed to the impulse force. This distinction means that the total amount of force overall is not important but rather the maximum peak that occurs during the impact.

THEORY

Initially the problem was looked at from a rigid body dynamics point of view with the forces described by Newton's laws. From Newton's first law, the ice is ideally considered to be in equilibrium as it floats on the water and moves with the current at a constant translational velocity and no rotational motion. Its velocity is taken to be the same as the water and it therefore has no relative motion to it. Using a reference axis on shore, I considered the bridge to be a rigid body at rest in the middle of the waterway with no motion.

Newton's third law states that for any force interaction between two bodies the second body always exerts an equal and opposite force to the first. The force that is measured at the model is therefore identical to the force experienced by the ice at the instant of impact. This force is the same regardless of how the impact is created; i.e., it is irrelevant if the ice moved into the bridge or the bridge moved into the ice.

The force created during this impact is determined by the mass of the bodies involved, their initial velocities, the acceleration that occurs during the impact and their velocities after the impact.

After the impact, if the solution of the linear velocity vector v and angular velocity vector ω of the two impacting bodies were possible, then the forces associated with the impulse of the impact could be determined by summing

$$\int_{t1}^{t2} \bar{F} dt = (m_i \bar{v}_{i2} + m_b \bar{v}_{b2}) - (m_i \bar{v}_{i1} + m_b \bar{v}_{b1}) \quad (1)$$

for the total linear momentum and

$$\int_{t1}^{t2} \bar{\Gamma} dt = (I_i \bar{\omega}_{i2} + I_b \bar{\omega}_{b2}) - (I_i \bar{\omega}_{i1} + I_b \bar{\omega}_{b1}) \quad (2)$$

for the total angular momentum. Since the ice and bridge are free to respond in three dimensions the determination of their velocities after the impact would be quite difficult.

The above also ignores the contribution of the water. The fluid in contact with the rear portion of the floe will decelerate and displace as it strikes the decelerating block. The fluid beneath the block is also accelerated as the block accelerates vertically into the fluid. These processes use energy and would need to be determined for an accurate energy accounting.

Furthermore, if frictional heating, fracturing or plastic deformation occurs to either body, some portion of the energy involved in the collision would be used in these processes and would be difficult to find analytically.

A useful relation for describing impulsive events is the coefficient of restitution e , which depends on the shape and material properties of the impacting bodies. The coefficient of restitution is defined as the ratio of the impulse force during restoration to the impulse during deformation for each body, or

$$e = \int_{td}^t F_r dt / \int_0^{td} F_d dt \quad (3)$$

where F_r is the contact force during restoration, F_d is the contact force during deformation, t is the total time of contact between the bodies, and td is the total time of deformation.

While the coefficient of restitution does not detail the local or internal behavior of the colliding bodies, it may be able to represent the behavior when determined either analytically or experimentally. It is, however, dependent upon velocity, as well as the material and body configurations. For perfectly elastic bodies with no energy loss, $e = 1$, and for perfectly inelastic bodies or plastic impact, $e = 0$ and the energy loss is at a maximum.

All of the above problems make an experimen-

tal determination of impact force desirable. They also point out the desirability of an accurate numerical technique to model impacts.

MODEL SIMILITUDE

The modeling procedure assumed that gravity forces were of primary importance. Thus to maintain dynamic similarity, the same ratio of inertial force to gravitational force from the model to the prototype was necessary. If the Froude number, defined as:

$$\sqrt{\frac{V^2}{Lg}} \quad (4)$$

where V is velocity, g is the gravitational constant and L is some convenient length, is a constant between the model and prototype, then dynamic similarity is achieved (Sharp 1981).

The pertinent similarity equations for the study were then

$$V_m = V_p (L_m/L_p)^{1/2} \quad (5)$$

and for the forces

$$F_m = F_p (L_m/L_p)^3 \quad (6)$$

where F is the force. The subscripts m and p denote model and prototype (full-scale) respectively.

With a 1/5th scale model study the above equations reduce to

$$V_m = 0.4472 V_p \quad (7)$$

and

$$F_m = 0.008 F_p \quad (8)$$

Since the prototype forces needed to be determined, the above equation was rearranged as

$$F_p = 125 F_m \quad (9)$$

EXPERIMENTAL PROCEDURE

The experiments were performed in CRREL's Ice Engineering Facility test basin. The basin is 36 m long \times 9 m wide \times 2.6 m deep and the room is capable of being cooled down to -20°C .

In the study some of the variables present in full scale were removed to cut down on the degrees of

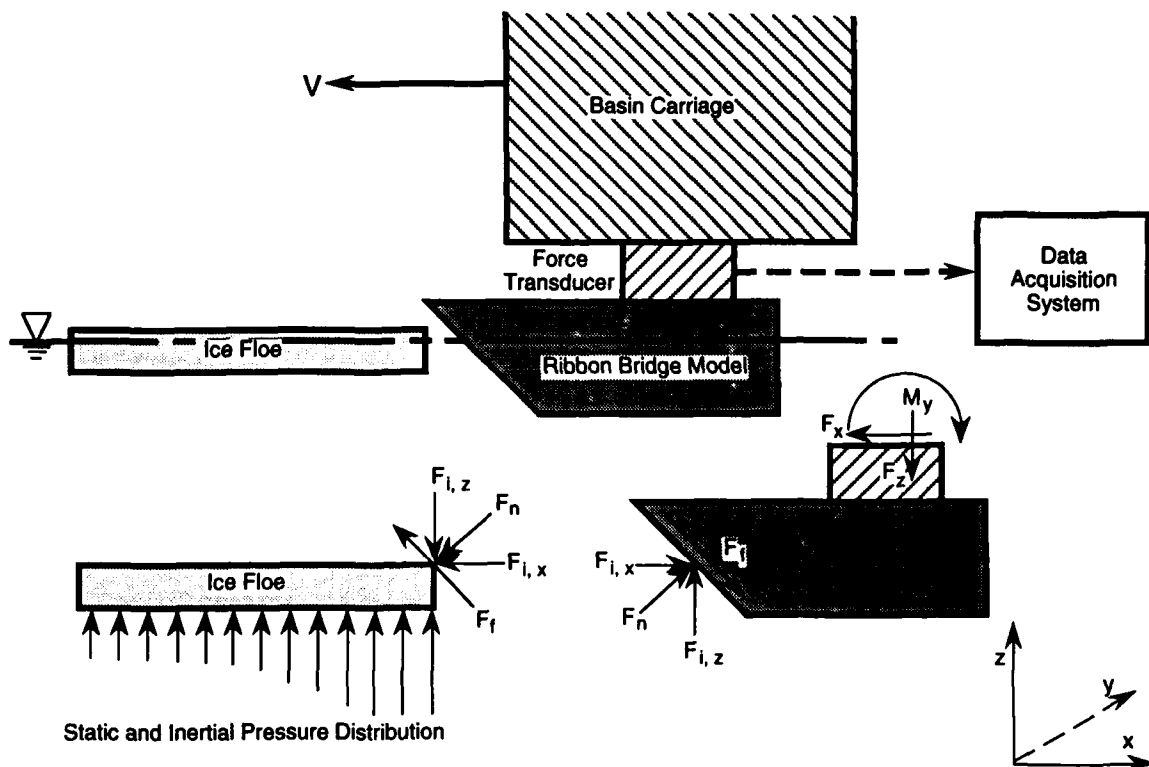
freedom for the problem. The bridge was assumed to be a rigid body, with no internal flexure and no external freedom to move vertically, or to rotate about a horizontal axis perpendicular to the ice motion. The ice floes were configured to impact squarely against the model, thus minimizing energy going into horizontal rotation of the floe. These precautions assured that the measured impact force would be conservative; i.e., it would model the highest force that is expected to occur naturally.

A heavily reinforced, 1.37-m-wide wooden model of a bow pontoon and a portion of a roadway pontoon were constructed. A thin steel skin was added to protect the face of the pontoon against ice abrasion. The bow pontoon provided the impact surface and the adjacent roadway portion of the pontoon helped to direct the fluid flow under the bow, thus avoiding any turbulence that might not be present in full scale (Fig. 2a). This configuration allowed us to determine impact forces against the pontoon but would not model forces at the connectors between bridge sections or pontoons.

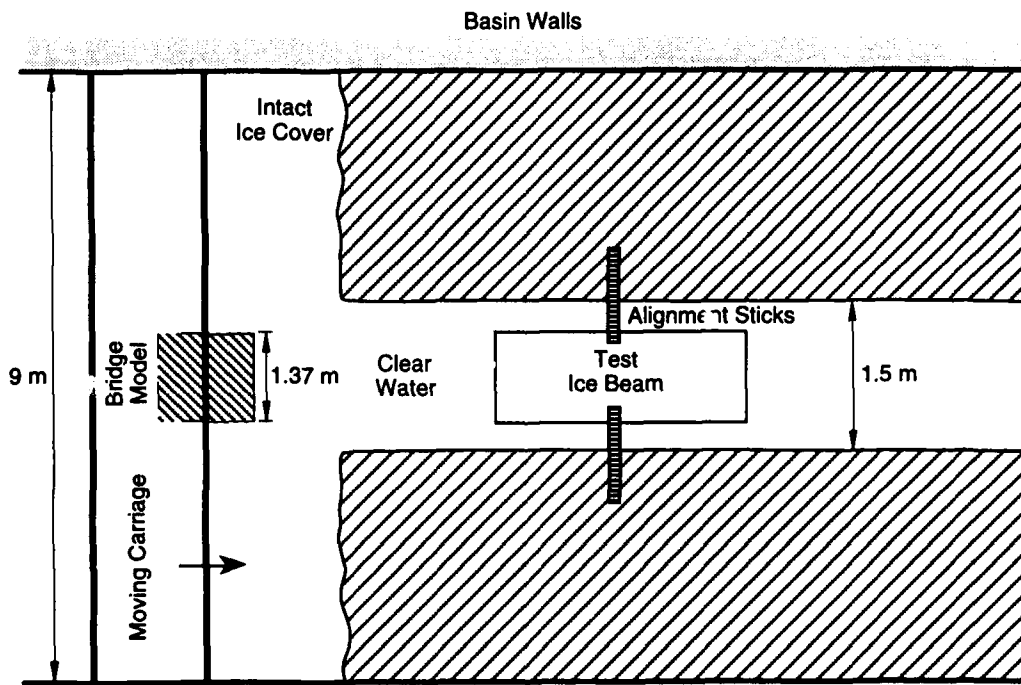
The top of the model was rigidly mounted, via a force transducer, under a moving carriage over the test basin. The transducer measured forces in three directions by sampling at a constant rate of 500 samples/second. The transducer analog output was converted to a digital signal and stored on a floppy disk. This allowed us to move the bridge into the ice and create an impulsive force equal to the naturally occurring situation where the ice is propelled into the bridge. Figure 2a shows a profile view of the test setup with the X, Y and Z directions indicated.

The floes were cut from freshwater ice in all combinations of four lengths and thicknesses, with a constant width of 1.37 m, as shown in Appendix B. The sizes were chosen to span a range that could be expected in field conditions. The model study represented prototype floes of 6.85-m width, with lengths varying from 1.52 to 15.24 m and thicknesses from 130 to 760 mm.

Only one size floe width was used because the force was assumed to be linearly proportional to width, as discussed later. The purpose of varying the lengths and thicknesses was to determine any effect, such as that of ice flexure or rotational under turning, other than the simple increase in mass of the larger floes. The impact tests were performed at four discrete model velocities in the expected range of prototype water velocities encountered in the field. The combinations of the above variables



a. Profile of bridge model, transducer and ice floe.



b. Top view of basin showing the basin carriage, ribbon bridge model and ice floe in the clear-cut slot in the ice.

Figure 2. Test setup. The model was driven at a constant velocity into the floating ice beam. In the free body diagram, forces are shown at the interface and at the transducer.

resulted in 64 tests, in one complete set. Four replicates of each test were planned, which resulted in a total of 256 tests. Some replicates and one test were not performed, so the actual number was 246.

The model ice sheets were normally grown by cooling the room air down below freezing until the desired thickness of ice was obtained. The exception to this procedure was the 152-mm-thick ice, which was obtained by stacking and freezing two 76-mm-thick ice sheets together.

A slot slightly wider than the model bridge was cut in the ice sheet, providing a clear path for the model to move in. A floe used in a particular test was placed in the slot and aligned parallel to the adjacent solid ice surface but still free to displace vertically and horizontally in the direction of impact. Two lightweight sticks were placed on both the floe and the ice sheet to hold the orientation of the floe before impact, as shown in Figure 2b.

PRELIMINARY TESTS

Preliminary tests were performed to determine the repeatability of the experimental results, to test the assumption that impact force varies linearly with floe width, and to test the effect of bridge displacement upon impact force.

Tests run to determine the repeatability of the experiments indicated a wide scatter in the results. Some of the floes were not impacting the bridge squarely and as a consequence some amount of energy was lost to floe rotation during these eccentric impacts. The repeatability of the tests was improved by designing the floes with a narrow nose. This resulted in a head-on impact and gave reasonably consistent impact loads.

The details of the preliminary work are given in Appendix A.

Although some discrepancy was noted in the data, an assumption of linearly varying force with floe width appears to be valid from the results of preliminary tests.

Bridge displacement had an effect upon impact force, with the largest variation being at the maximum displacement tested. At this displacement, the average force in the longitudinal direction had a 9% drop, while the average Z-force showed a 31% average increase over the lower two displacements tested. The majority of tests were run at this maximum displacement of the model bridge, to have a conservative value for the vertical forces while the longitudinal force values are perhaps 10% low in the worst case.

NUMERICAL PROCEDURE

A finite element analysis was performed using a combination of ABAQUS software (Hibbitt, Carlson and Sorenson Inc. 1989) for the solid mechanics (ice and bridge) portion and a fluid influence coefficient matrix to account for the influence of the fluid inertia (McGilvary et al. 1990). The ice beam was modeled using beam elements which use Euler-Bernoulli beam theory; i.e., any transverse shear deformation is ignored, with a cubic interpolation of displacement. The numerical beam was split up into 30 elements with a variable nodal spacing along its length. A dense nodal spacing was used in the impacted end of the beam, gradually becoming less dense by a factor of 5% per node towards the opposite end of the beam.

The bridge was modeled as a massless, 45°-sloped, rigid surface using an element that allows vertical and horizontal displacement but no rotation. Variable displacement stiffness is incorporated by attaching massless springs to the surface, as shown schematically in Figure 3. The spring stiffness was calculated by utilizing the measured free vibration frequency of the bridge model, an estimate of the effective mass of the bridge, and the natural frequency equation:

$$f = \sqrt{k/m} / 2\pi \quad (10)$$

where f = the oscillation frequency

k = the spring stiffness

m = the mass of the bridge.

An average oscillation frequency of 13.5 Hz was measured and, with an estimated mass of 34 kg for the bridge model, gave a value of 250,000 N/m for the stiffness of the surface support in the majority of the numerical runs. The ice elastic modulus was 2.0 GPa and it was assumed to be isotropic. A series of numerical runs using 152-mm-thick ice were performed to test the effect of structure stiffness and ice elastic modulus on impact force. In these, the spring stiffness was doubled to 500,000 N/m, to study structure stiffness, and the ice elastic modulus was increased to 10 GPa, which corresponds to a hard freshwater ice (Ashton 1986).

The static portion of the fluid pressure beneath the ice is defined as a distributed elastic foundation (Winkler foundation) by a series of springs at each beam node. These springs have a nonlinear spring stiffness, shown in Figure 4, to simulate the changing static fluid pressure on the ice (buoyancy force) when it displaces from equilibrium.

The dynamic influence of the fluid is calculated

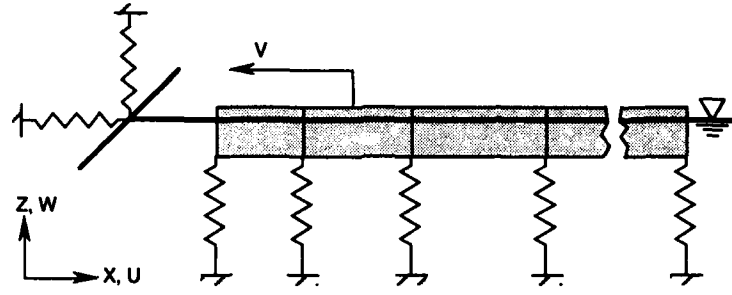
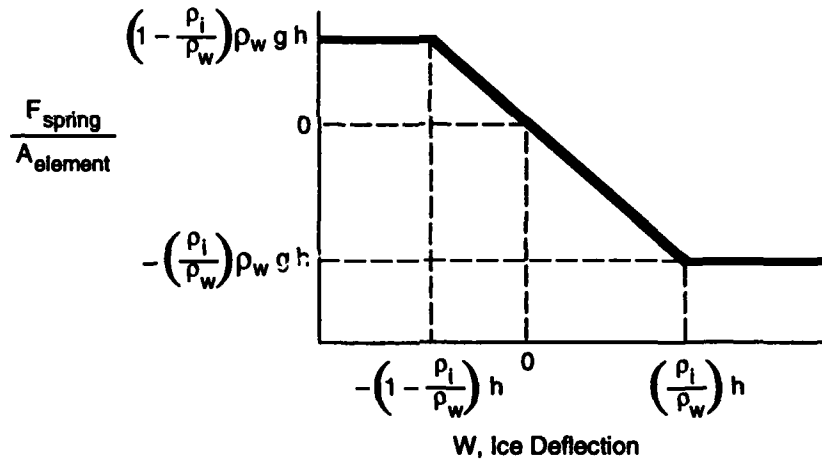


Figure 3. The finite element model of the bridge and ice beam. U is horizontal displacement and W is vertical displacement. The fluid foundation is represented by massless springs.

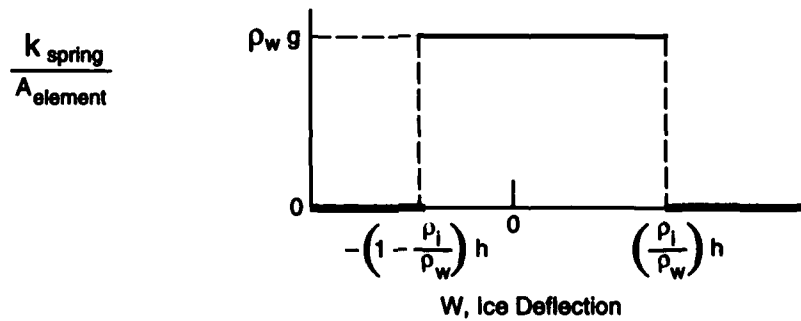
in a separate finite element procedure. In this, the fluid domain of the flume is discretized into finite elements with an area corresponding to the ice beam on top. Through the wave equation

$$\frac{1}{c^2} \frac{d^2 P_a}{dt^2} - \nabla^2 P_a = 0 \quad (11)$$

where c is the speed of sound and P_a is the acoustic pressure. By ignoring the first term as very small, the acoustic pressure that is caused by a unit acceleration of each succeeding ice node, in turn, while the others are held at zero, is calculated for each node in the fluid grid. The acoustic pressure



a. Static foundation reaction force.



b. Foundation modulus with respect to displacement.

Figure 4. Plots of static foundation reaction force and foundation modulus with respect to displacement, for an ice node. ρ_i is ice density, ρ_w is water density, h is ice thickness and g is the gravitational constant.

values at the fluid/ice interface are then multiplied by the area of the ice over which they act, giving an inertial force at the interface. This inertial force is then divided by the unit acceleration to give a fluid added mass, at each ice/water interface node. The resulting value of added mass for each node is the fluid influence coefficient matrix. This fluid influence coefficient matrix is then added to that of the ice beam in the numerical model, where its multiplication with the ice beam accelerations yields the fluid inertial forces acting on the ice. More detail on the fluid inertial formulation can be found in (McGilvary 1989).

BEAM RESPONSE

To assess the ability of the model to simulate an impulsively loaded, floating beam, a series of tests were done to measure the response of a floating ice beam to a vertical impulsive force at one end. The beams were either 54 or 60 mm thick and 305 mm wide. The lengths varied from 2 up to 30 m and typically had two free ends. The characteristic length of the ice is a way of expressing the magnitude of ice stiffness to foundation stiffness. It was determined by first measuring the displacement caused by placement of a 1-kg dead weight on a representative ice beam and using the following formula (Hetenyi 1946):

$$w = \frac{PL_c}{2KB} \quad (12)$$

where w is the end deflection of the beam caused by the load P at the end, K is the foundation modulus, in this case the specific weight of water (Ashton 1986), and B is beam width.

The elastic modulus, E , was calculated from this by applying the theory of an elastic beam on an elastic foundation with the following formula (Hetenyi 1946):

$$L_c = (Eh^3/12K)^{1/4} \quad (13)$$

where E is the effective elastic modulus and h is the ice thickness.

The value of L_c was found to be 2.68 m and E to be 1.72 GPa.

The floating ice beams were instrumented along their length with five linear variable-displacement transducers (LVDTs). Typically, one LVDT was placed at the impacted end, one about 1 m back from the impacted end, one in the middle at the beam, one halfway between the middle and the far end and one at the far end. A vertical impulsive load was applied to one end by a wooden dowel, instrumented with a load cell. Figure 5 shows schematically a typical test arrangement. After the short duration load was applied, the free vibrations of the beam were recorded by the LVDTs.

Figure 6a shows a typical force-history trace

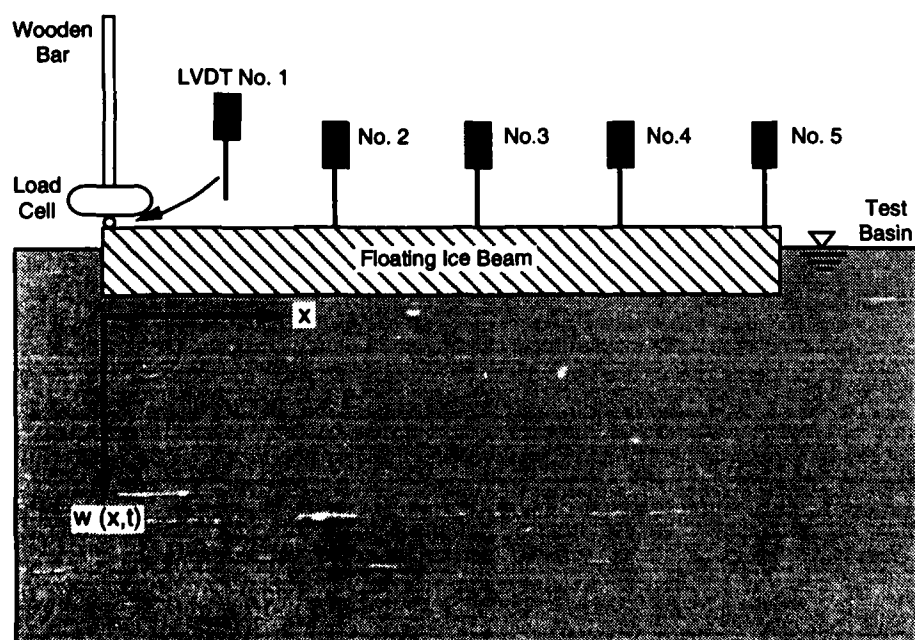
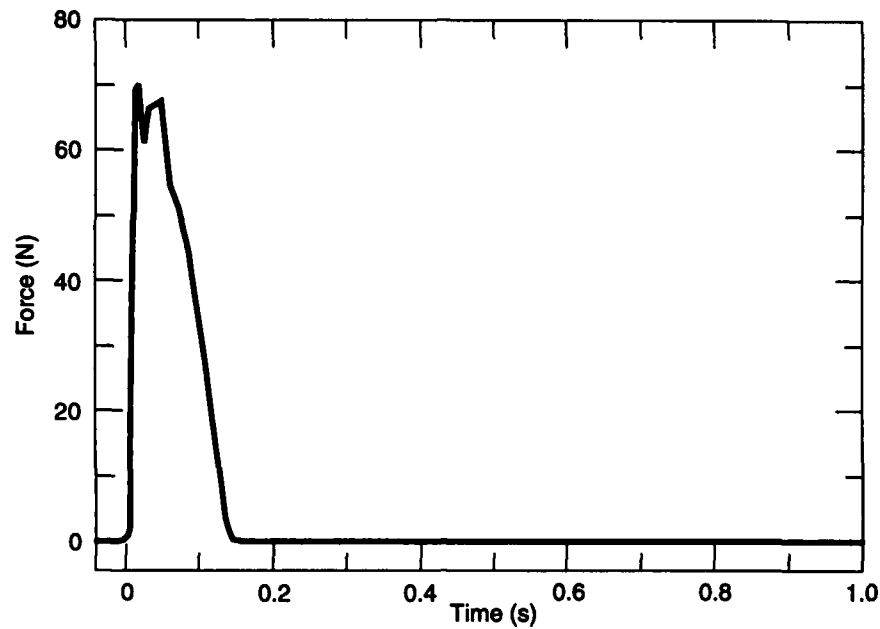
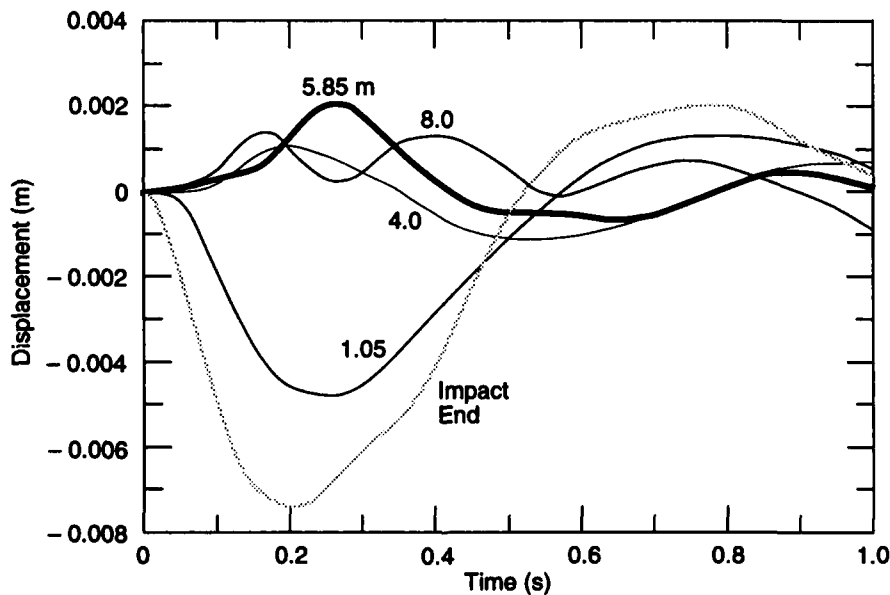


Figure 5. Schematic diagram of a floating ice beam instrumented with LVDTs. An impulsive load is applied at the end by the bar and measured by the load cell.



a. Force-history plot.



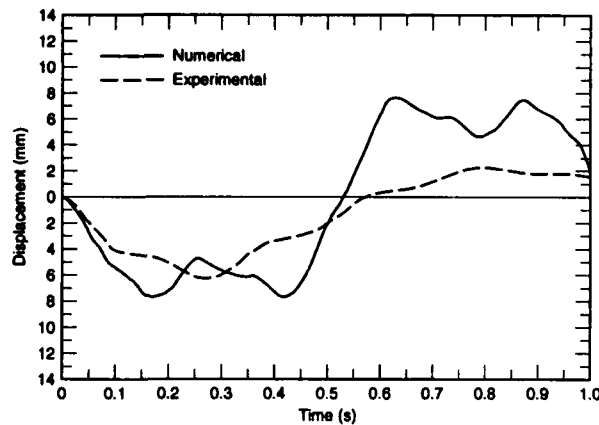
b. Displacement histories at different points on the beam.

Figure 6. Typical results from an 8-m-long beam response experiment.

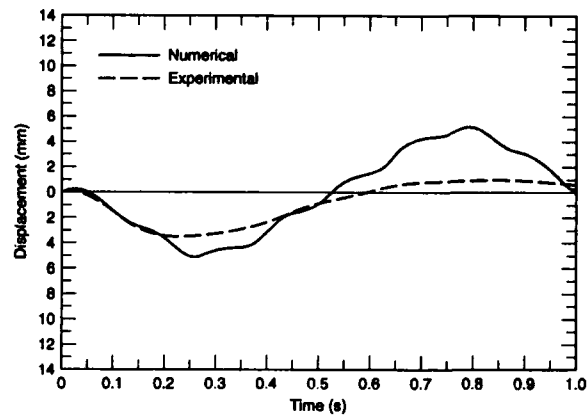
created by the applied vertical impulsive load, and Figure 6b shows the measured response of the beam at several distances. The force typically rose monotonically for 0.03 to 0.07 s to its peak value and then decreased monotonically at a somewhat slower rate to zero. Overall the force histories were relatively symmetrical about the peak value. It can be seen in Figure 6b that the impact end of the

beam exhibited the largest displacements over time, as expected. The displacements further along the beam show a slight time lag from the maximum displacement at the impacted end as well as smaller displacements as the impulsive energy is lost to the beam and supporting fluid.

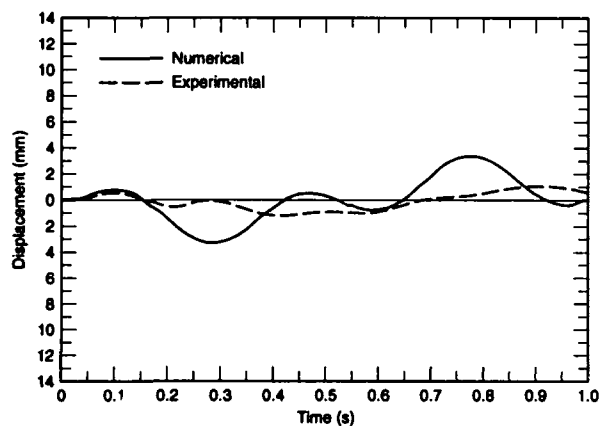
Figure 7 shows a comparison between the experimental and numerical displacement data for a



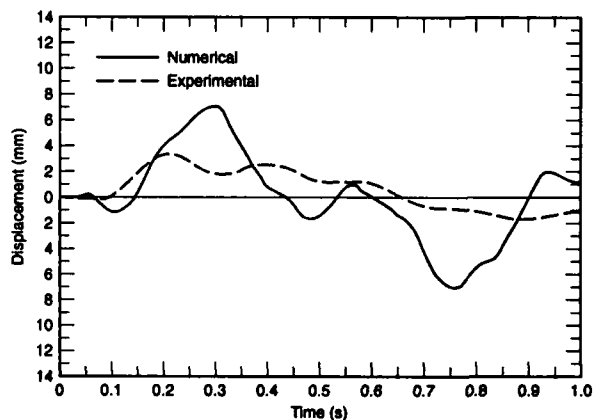
a. At the impact end.



b. 1.05 m from the impact.



c. 2 m from the impact.



d. 4 m from the impact.

Figure 7. Comparison of numerical and experimental beam displacement histories for a 4-m-long beam.

4-m-long beam. Comparisons of theoretical and experimental responses of 8-m-long and 15.25-m-long beams are shown in Figures 8 and 9, respectively. The model increasingly overpredicts the measured deflections at points farther from the loaded end of the beam. If one point on the beam is observed and time allowed to progress, the numerical model shows the best agreement in the first 0.5 second. In other words, the greatest discrepancy between the numerical and experimental data occurs at the end of the beam farthest from the impact or after the first 0.5 s. This is understandable, because any vibrating floating body will transfer kinetic energy to the fluid mass by generating surface waves, and the numerical model does not account for this energy transfer.

The numerical model also assumes elastic behavior for the ice and complete energy conservation. This means that there is no loss of energy due to internal dissipation. It also means that the propa-

gating flexural waves reflect off the ends of the numerical ice beam, with no loss to the fluid or atmosphere. One of these reflected waves is evident in Figure 7a at about time 0.25 s.

Despite the shortcomings noted above, the numerical model shows good agreement with the experimental data. Furthermore, for impulsive force measurements, only the ice response during the impact is of concern. This is the portion of the event, temporally, where the numerical model shows the best agreement with the experimental data.

EXPERIMENTAL RESULTS

A typical impact force/time record is shown in Figure 10. The X-direction (along the axis of impact) force is on the top, the Y-direction (transverse to impact) is in the middle and the Z-direction

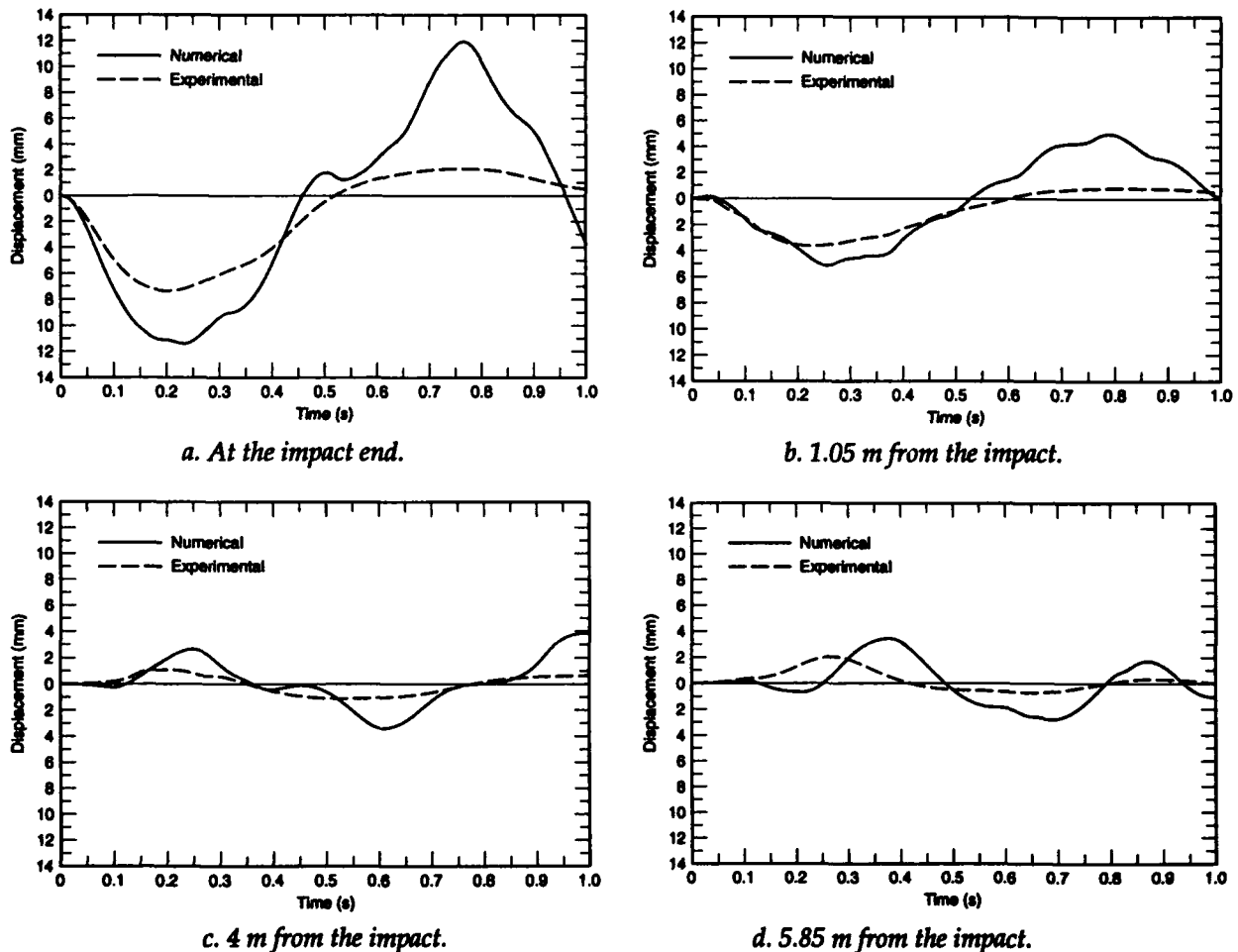


Figure 8. Comparison of numerical and experimental beam displacement histories for an 8-m-long beam.

(vertical) is the bottom curve.

An upward force on the bridge is represented by a downward Z-force trace. The bottom line represents the carriage speed. It was included to confirm that the carriage speed was essentially constant before the impact event.

A look at Figure 10 is informative to understand the impact event. The X-force trace (top) shows, just after the impact peak, that there is a small dip in the trace where the force falls below its pre-impact value, as the beam rebounds off the face. This dip may be caused by bridge's rebound after the impact, or because there is a momentary pause before the water fills in behind the rebounding beam. The trace then flattens as the bridge continues through the water, until catching up to the rebounded beam. Only the peak values of the first impact are used in this report. The peak value was measured from an average value calculated several seconds before the impact.

The Z-force trace was similar with the exception of the model's behavior between the first and second impacts. It can be seen from the Z-force trace there is a sinusoidal vertical forcing that appears after the first impact. This may be caused by the surging of the water as it fills the void left by the beam after the first impact or perhaps it is the free response of the bridge after the impact.

The Y-force is near zero as it should be in a properly aligned impact. Some vibration in this direction is evident shortly after the X direction peak impact.

The data on maximum total ice force for different beam thicknesses and lengths are presented graphically in Figures 11–14, beginning with the measurements at the lowest impact velocities. The magnitude of the total force was calculated by adding the horizontal and vertical components vectorially. The tabulated values are given in Appendix B.

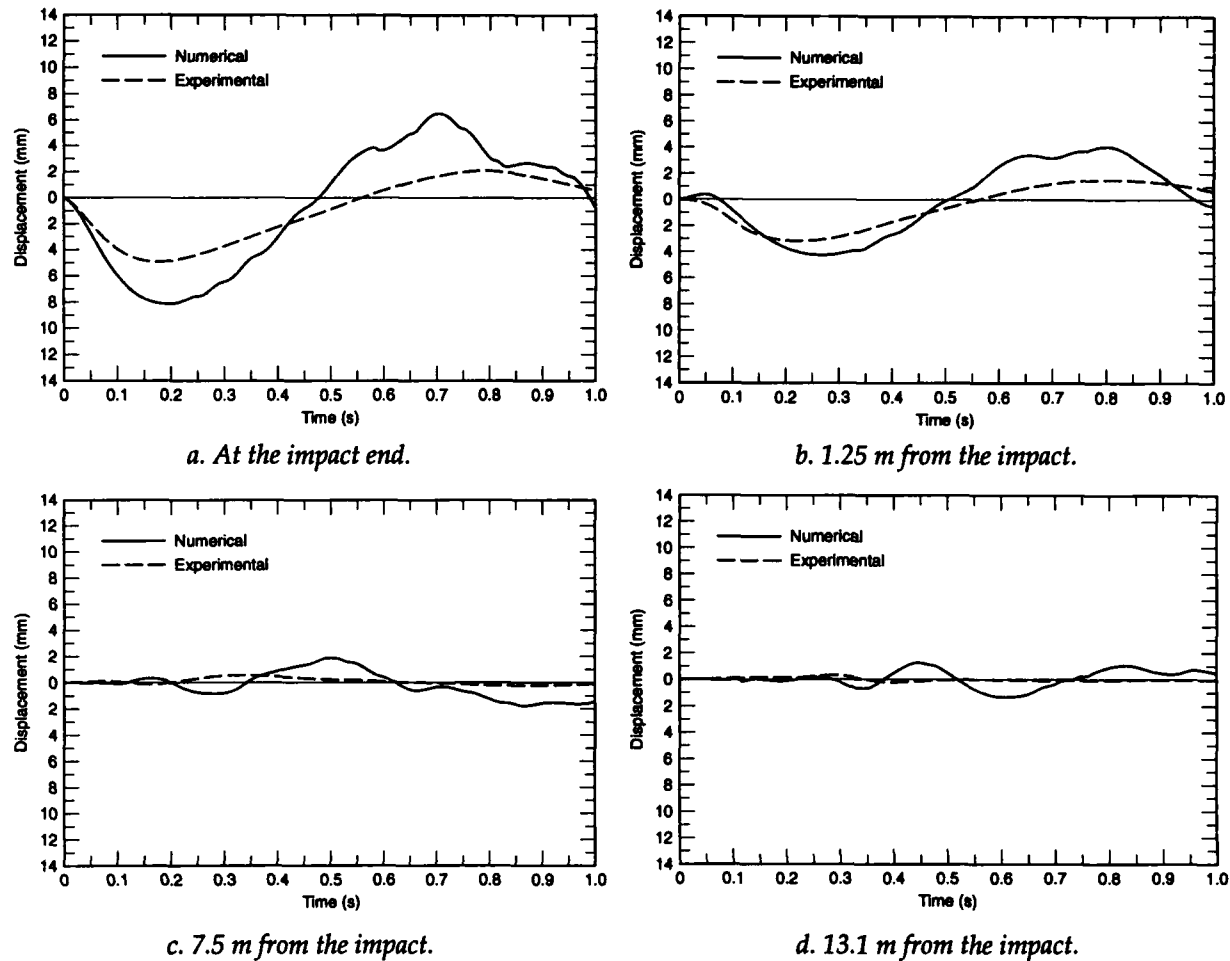


Figure 9. Comparison of numerical and experimental beam displacement histories for an 15.25-m-long beam.

Equation 9 was used to obtain prototype values of impact force from the results of the model tests and these values are also given in Appendix B.

Figures 11–14 show that the peak impact force increases monotonically with increasing velocity and beam length, until finally exhibiting a tendency to level off and approach a constant value for long beams and higher velocities. This phenomenon is quite evident from the test results using thin beams. As beam thickness increases the leveling off effect is not significant until the length or velocity increases to a threshold level. An inspection of the X and Z forces separately indicates that this trend holds in both those directions as well as for the total force.

A long thin beam would exhibit this trend at a lower velocity than a short thick beam because of a thin beam's tendency to absorb energy through flexure, while a short thick beam acts more as a rigid body, which is consistent with the data. The

results from the thickest beams did not exhibit this trend at a velocity of 0.1524 m/s regardless of the beam length. Some reduction of force barely manifests itself at 0.6096 m/s and can be seen rather well at 1.0668 m/s. Unfortunately data for a 2.1-m-long beam at 1.524 m/s are not available, and this makes it difficult to see the trend in Figure 14.

In the absence of friction, bridge inertia, and any effect from fluid drag, the X and Z component forces would be equal in magnitude. In the experiments, however, the X-forces are on the average 39% greater than the Z-forces. Figure 15 is a graph of X-force versus Z-force. The solid line is the best fit regression line through the points. If the difference in the component forces is due to friction, the coefficient of friction (μ) can be calculated by

$$\mu = \tan(\phi) \quad (14)$$

where ϕ is the friction angle. For the data ϕ is 8.30,

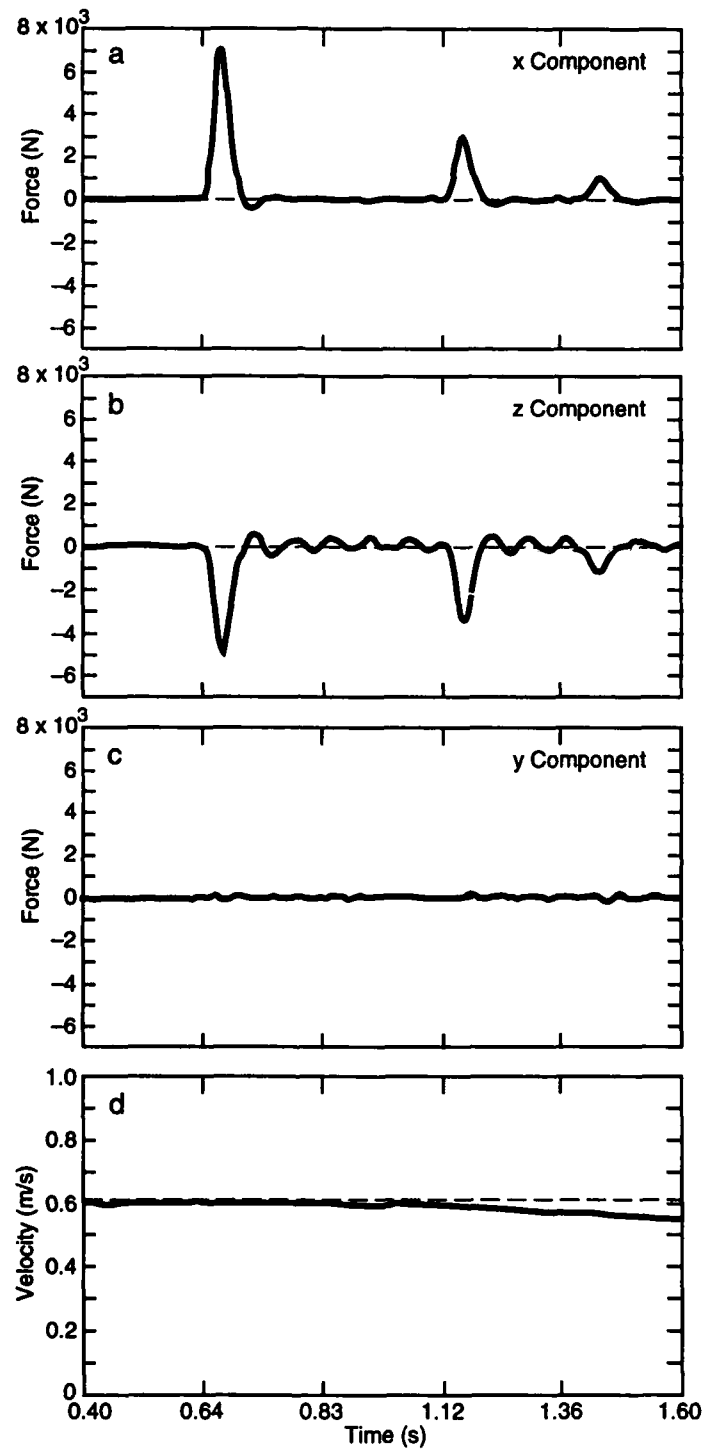


Figure 10. Typical plot of force vs. time data from the experiments. In this case, the initial impact occurs at 0.64 s.

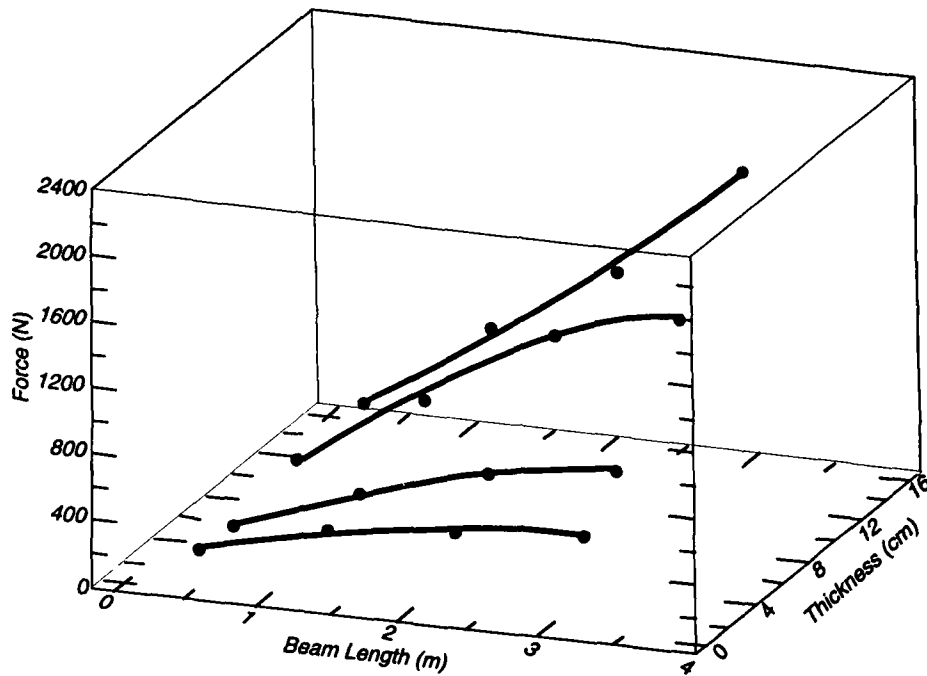


Figure 11. Average peak impact force vs. beam length and beam thickness, for the replicated experiments, at 0.1524 m/s.

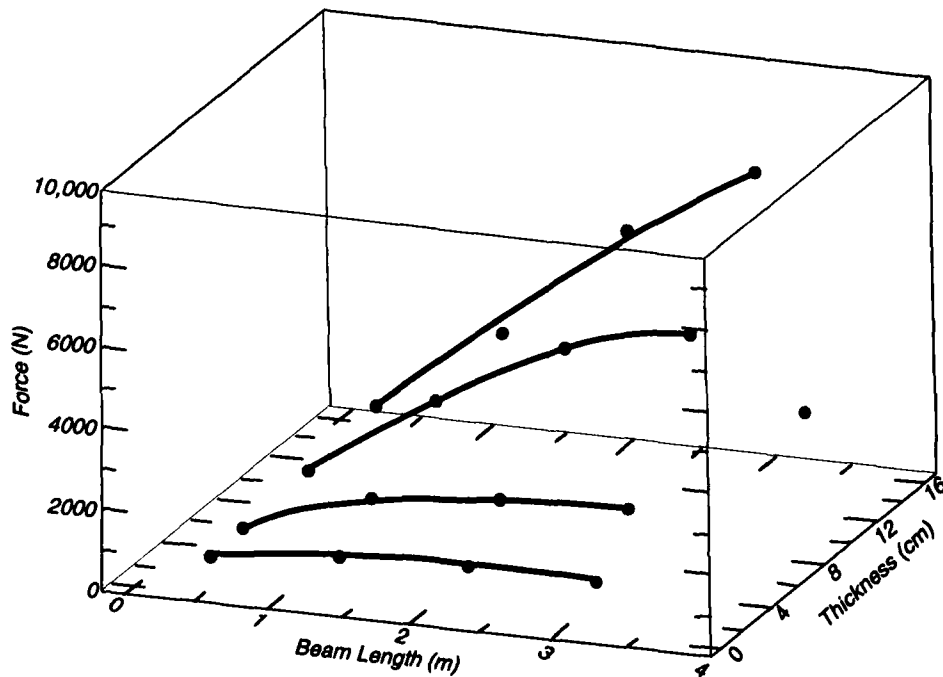


Figure 12. Average peak impact force, vs. beam length and beam thickness, for the replicated experiments, at 0.6096 m/s.

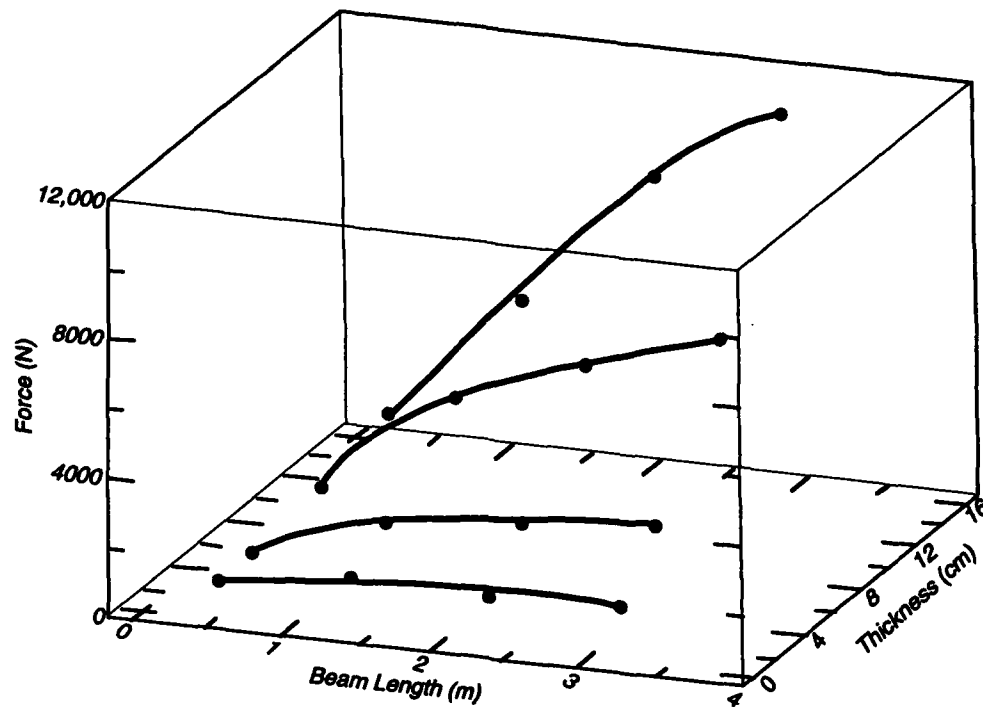


Figure 13. Average peak impact force, vs. beam length and beam thickness, for the replicated experiments, at 1.0668 m/s.

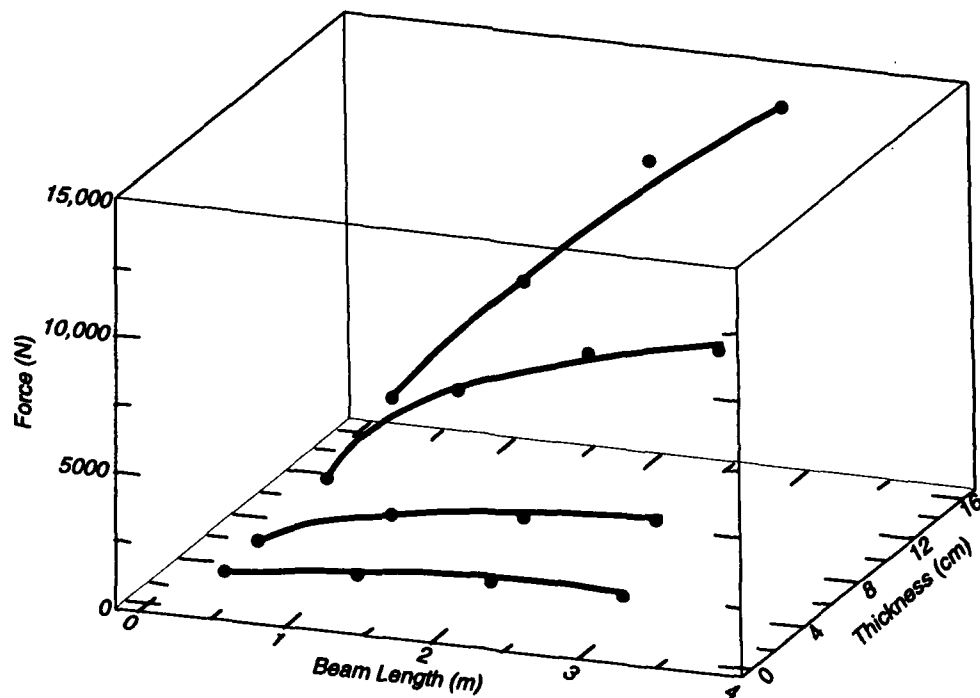


Figure 14. Average peak impact force, vs. beam length and beam thickness, for the replicated experiments, at 1.524 m/s.

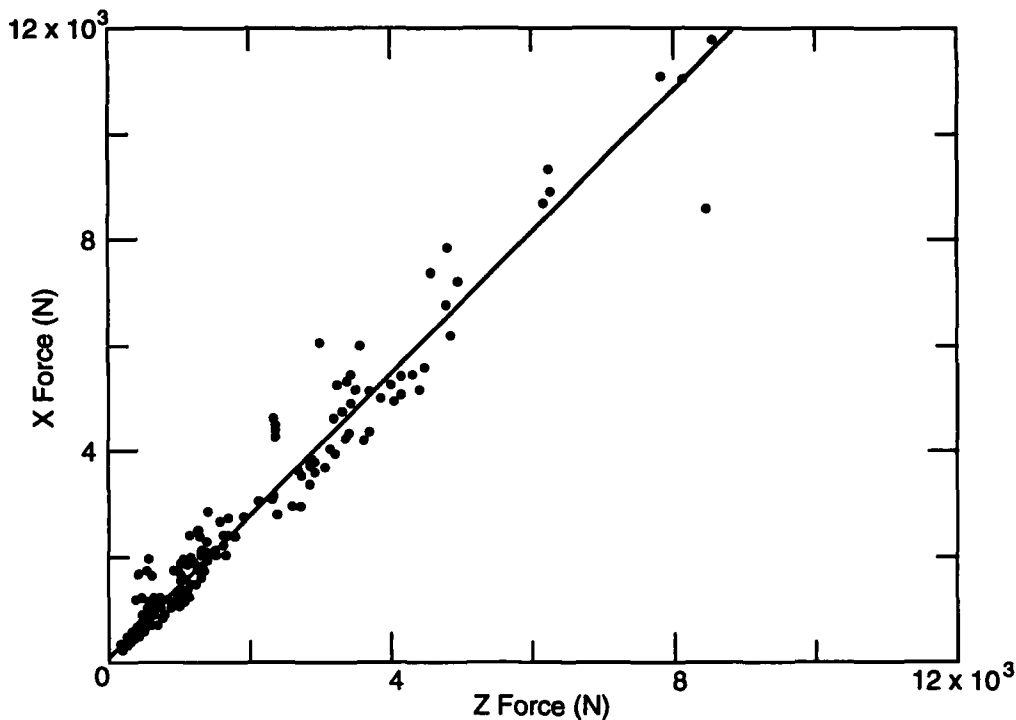


Figure 15. Maximum values of F_x vs. F_z , showing a constant ratio of F_x/F_z to be approximately 1.34. This yields a friction angle of 8.3° and a friction coefficient ($=F_f/F_n$) of 0.15.

which gives a value of μ of 0.15. This value of μ has been shown to be possible between ice and stainless steel, especially when the stainless steel roughness was increased (Forland 1985). In the same report it was also shown that μ could increase with velocity.

The trend in the data is not uniform and exhibits a rough correlation with velocity. For any given beam size the X-force is closest to the Z-force at 0.1524 m/s. In some instances the Z-force is actually greater than the X-force at this velocity.

In general, as the velocity increases the X-force becomes increasingly larger than the Z-force. The notable departures from this trend are the beams with lower length to thickness ratios. During the impacts described earlier, it was easier for short, thick beams to rotate, in comparison to longer beams. The resulting movement in the Z direction required the beam to displace the water beneath it. At impact these unstable beams reacted along the path of least resistance (i.e., in the X direction) and therefore generated less Z-force against the 45° sloped surface. This is discussed later in this report.

It was speculated that the increase in X-force might be associated with the increase in viscous

drag caused by the sudden acceleration of the beam through the water at impact. To obtain the drag force associated with the sudden acceleration of a flat plate, the shear force per unit area is first calculated by

$$\tau_{zx} = -\mu \frac{dv_x}{dz} \quad (15)$$

where τ_{zx} = the shear stress in the X direction caused by fluid in the Z direction (perpendicular to the plate)

μ = the fluid viscosity

v_x = the X-component of the fluid velocity (Bird et al. 1960).

In order to do this calculation, an estimate of the thickness of the fluid momentum boundary layer is needed. This boundary-layer thickness δ is approximated by

$$\delta = 4 \sqrt{\nu t} \quad (16)$$

where t is time and ν is the fluid kinematic viscosity

$$\nu = \frac{\mu}{\rho} \quad (17)$$

Table 1. Fluid drag forces associated with the sudden acceleration of a flat plate for each size ice beam calculated at the highest and lowest experimental velocities. The last column is the percentage of average X-force the drag force comprises.

<i>Beam length (m)</i>	<i>Velocity (m/s)</i>	<i>Beam thickness (m)</i>	<i>Fluid drag (N)</i>	<i>Percentage of average X-force</i>
3.05	0.1524	0.0254	11.37	4
3.05	1.524	0.0254	113.8	14
3.05	0.1524	0.1524	11.37	1
3.05	1.524	0.1524	113.8	1
2.134	0.1524	0.0254	7.95	3
2.134	1.524	0.0254	79.61	10
2.134	0.1524	0.1524	7.95	1
2.134	1.524	0.1524	79.61	N/A
1.219	0.1524	0.0254	4.54	3
1.219	1.524	0.0254	45.47	8
1.219	0.1524	0.1524	4.54	1
1.219	1.524	0.1524	45.47	1
0.305	0.1524	0.0254	1.14	3
0.305	1.524	0.0254	11.38	5
0.305	0.1524	0.1524	1.14	1
0.305	1.524	0.1524	11.38	1

with ρ the fluid density (Bird et al. 1960). It is evident from eq 16 that the boundary layer thickness is proportional to the square root of time. In the calculations of the fluid drag during the impact events, the rise time of the force was used in this calculation. The rise time is the time from the beginning of the impact to the time of maximum peak force measured from the experimental force time histories. This time was relatively consistent and an average of 0.05 s was used in eq 16. This gave a boundary layer thickness of 0.01 m. To parametrically bound the values, the shear stress was calculated for the highest velocity of 1.5 m/s and lowest velocity of 0.15 m/s. The stress values from these calculations were then multiplied by the beam surface area to arrive at a final drag force value for a given size beam at each of the above velocities. This value was then divided by the average X-force value at the same conditions to determine the percentage of the X-force that could possibly come from drag. The results are listed in Table 1.

Table 1 shows that this drag force accounts for less than 15% of the total X-direction force in the best case. The surface roughness of the ice is not considered in this calculation. An ice beam is probably rougher and might generate greater shear stress than what the flat plate model provides, but it is unlikely that it could account for the difference

between 15% and the measured 39% difference.

During the experiments it was noticed that the bridge face had become dented. This denting could have changed the local geometry enough to present a more vertical face to the impacting ice thus causing higher X-direction forces.

Another possible explanation for the higher X-forces might be a dynamic interaction of the model during beam impact. The configuration of the model and transducer relative to where the ice impacted the model could cause this interaction to show up more in the X-direction than in the Z-direction.

RESULTS AND DISCUSSION

Figure 16 shows a typical force versus time record for a 1.219-m-long, 152-mm-thick, 1.37-m-wide beam from the numerical program. Since the bridge is modeled as a massless structure, the force versus time record is symmetric with no effect of bridge inertia evident in the impact. The force values used in the comparisons below were the maximum impact force corresponding to the apex of the trace.

Figure 17 shows comparisons between the numerical peak impact force and the average experimental peak impact force, versus ice beam length,

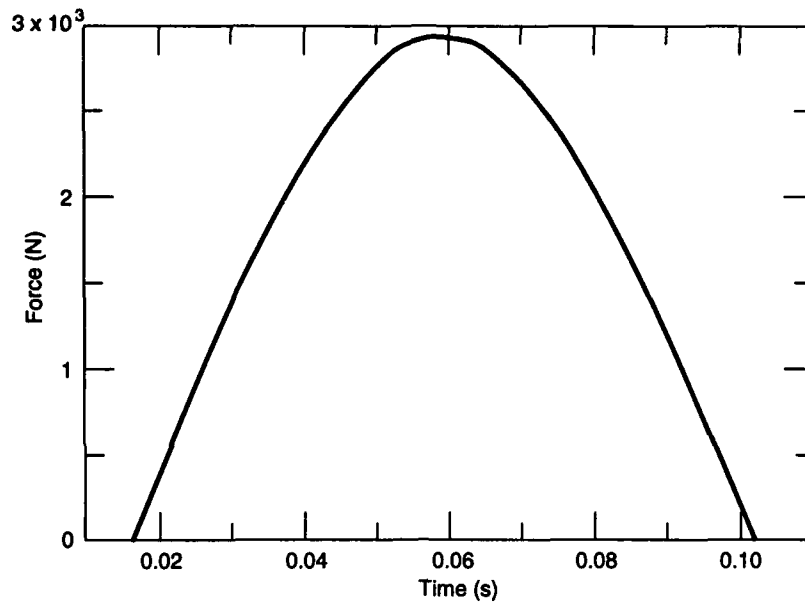


Figure 16. A typical numerical force vs. time plot from an impact of a 1.219-m-long beam at 0.61 m/s.

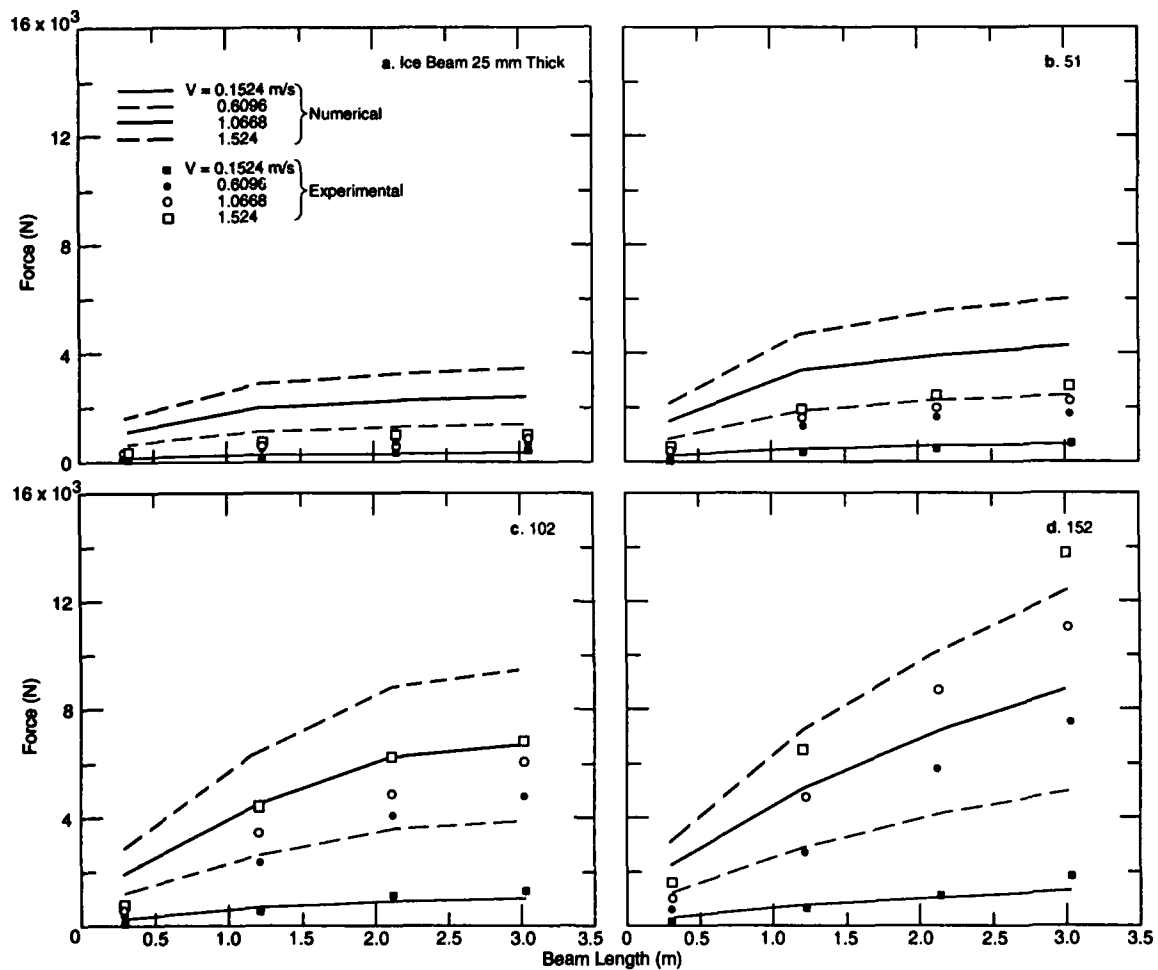


Figure 17. Comparisons of average, experimental, peak impact force, and numerical, peak impact force vs. ice beam length, at constant velocities, for a given thickness ice beam.

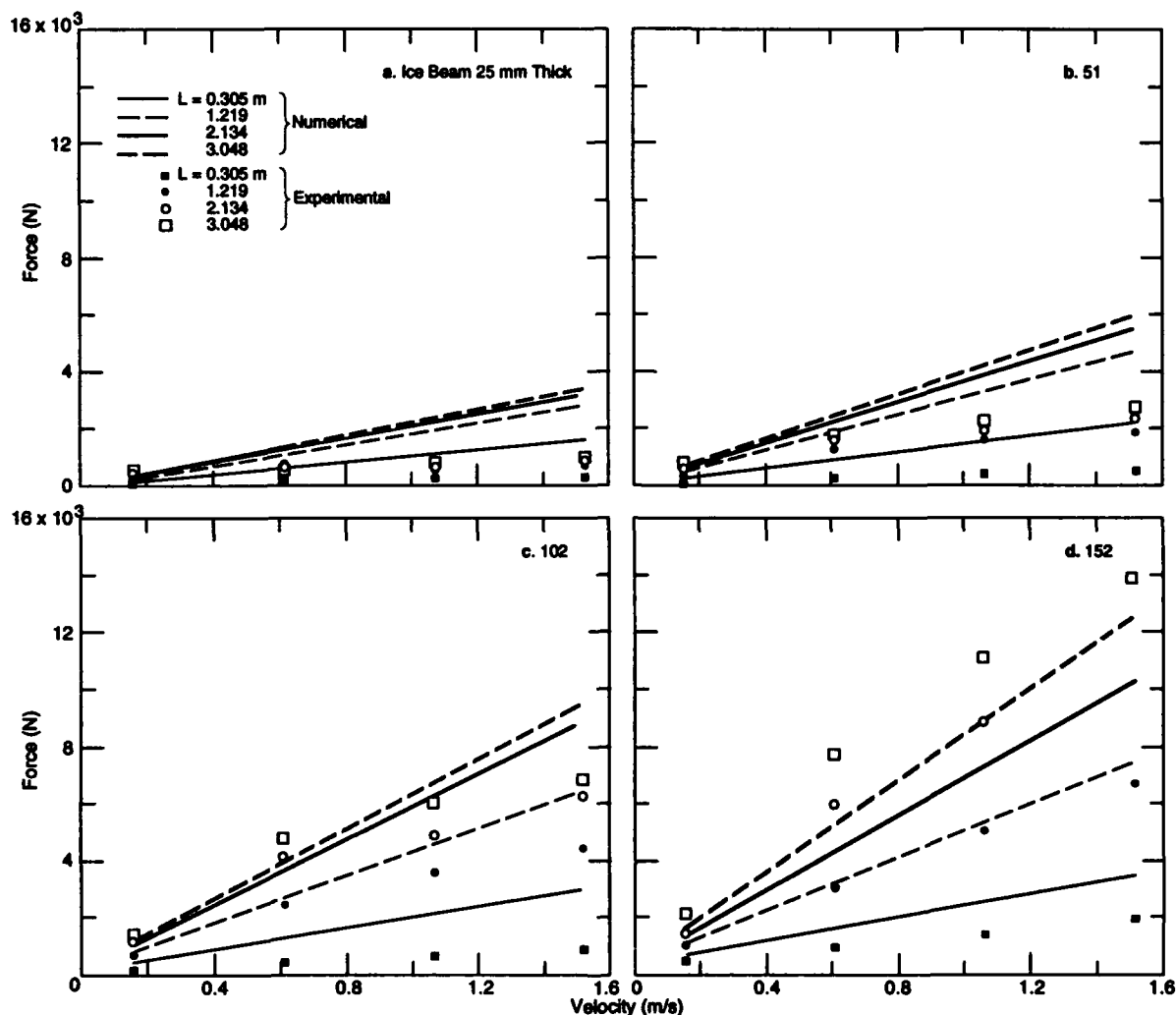


Figure 18. Comparisons of average experimental peak impact force, and numerical peak impact force vs. impact velocity, at constant beam lengths, for a given thickness ice beam.

at constant velocities, for each experimental ice thickness. It can be seen here that the numerical and experimental forces exhibit the same tendency to approach a constant value as beam length and velocity increase.

In Figure 18, comparisons between numerical peak impact force and average experimental peak impact force, versus impact velocity at constant beam length, are shown for each experimental ice thickness. Here it appears that the impact force from both the numerical and experimental 0.305-m-long beams, when plotted against velocity, exhibits a different trend than that of the other beam lengths. Generally, the slope of the curve for the 0.305-m-long beam is flatter than those of the other beam lengths, and the force magnitudes appear to be noticeably lower.

In both figures, the numerical force is higher than the experimental force for the thinner ice at all but the lowest velocities, becoming closer to the experimental force as the ice thickness increases. This is understandable, since numerically the ice is treated as an elastic body, with no failure criteria, with the energy completely conservative. In the experiments, the thinner ice was easier to damage, especially as the velocities increased, which means the experimental forces would not be as high as the numerically modeled forces. Most of the damage in our experiments took the form of either cracks propagating back from the nose of the beam, or pieces of the beam fracturing and breaking off. Appendix B lists the damage noticed in the experiments.

The forces generated during the ice impact

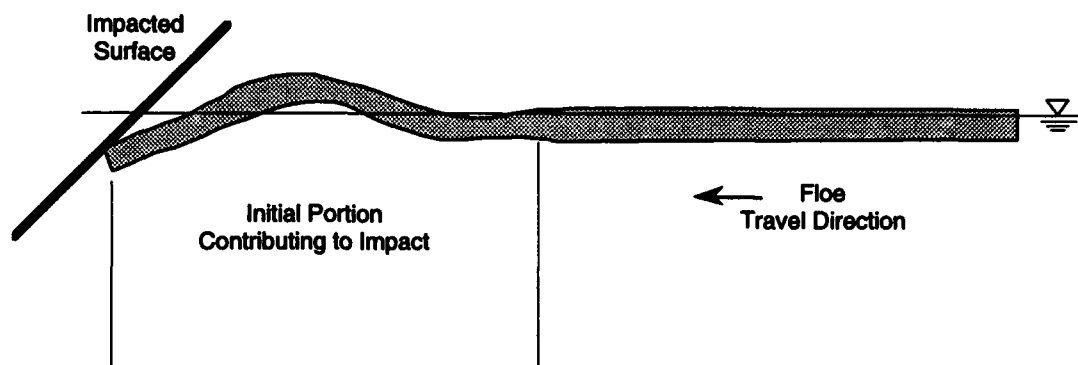


Figure 19. During impact, only the initial portion of an ice beam will contribute to the impact force as illustrated above. The size of the portion that contributes to the impact will depend upon the length and characteristic length of the ice beam.

events depend upon factors such as the mass of the bodies, the impact velocity, the post-impact velocities of the bodies, the internal dissipation of energy in the bodies, and the energy lost to the supporting fluid during the impact.

For the experimental impacts where the ice beams broke and fractured, the impulsive force recorded would be lower than what a pure elastic body would have generated because of the energy used during fracturing. In the impacts where the beams did not break, a linear force increase according to Newton's second law was expected. As Figure 17 shows, however, the forces tended to approach a constant value with increasing beam length. This trend is also evident in the numerical data, so it is not solely related to energy used in damaging the ice.

This trend could be related to the characteristic length of the ice, which would imply that impact force will approach a constant value when the beam length is more than some multiple of the characteristic length. Any length increase beyond this multiple will not contribute to the impact force, as only the front part of the beam will react during the impact. This is illustrated in Figure 19. If this supposition is correct then it should be possible to nondimensionalize and scale the data with respect to the characteristic length.

The characteristic lengths of the ice beams are listed in Table 2. These were calculated using eq 12 and 13.

Figure 20 shows comparisons between nondimensionalized numerical and experimental impact force, versus beam length divided by characteristic length (L/L_c) at constant velocities. The force is nondimensionalized by dividing by the effective volume of the beam, which is calculated

using the beam's characteristic length, multiplied by the acceleration of gravity and the density of water. This results in a nondimensional force value that has the effective mass of the beam incorporated in it. The effect of beam thickness is also illustrated within each figure.

The nondimensional numerical force does tend to approach a constant value with increasing L/L_c as Figure 20 shows. The forces from the 0.305-m-long beams (low L/L_c values) are consistently higher than the other length beams at similar velocities. The experimental forces overall are lower than what is predicted by the numerical data. This is expected because the experimental ice beams could be damaged during impact while the numerical beams are modeled as pure elastic bodies. The differences between the numerical predictions and measured experimental forces were less at the lowest velocities, where damage to the experimental beams was less likely to occur.

A comparison of the experimental and numerical nondimensional force data shows overall a much flatter trend of force vs. L/L_c in the experimental data. The force increases more steeply at lower L/L_c values and then tends to flatten out with increasing L/L_c , in the experimental data, for all but the 25-mm-thick ice. The force then tends to approach a constant value in much the same manner as the numerical force, except with a lower

Table 2. Beam thickness and associated characteristic length for the test beams.

Thickness (m)	0.0254	0.0508	0.1016	0.1524
L_c (m)	0.70	1.18	1.98	2.68

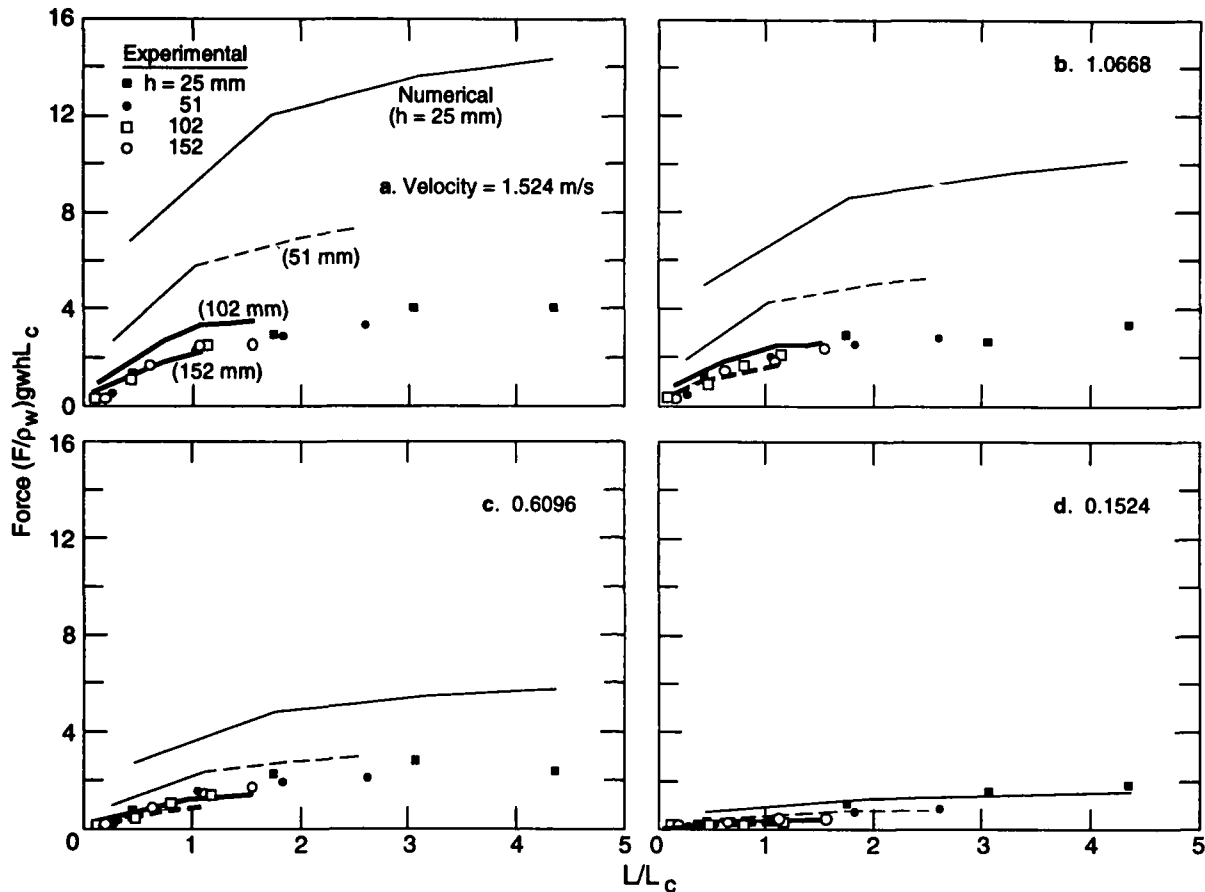


Figure 20. Comparisons of nondimensional experimental and numerical impact force, vs. beam length divided by characteristic length (L/L_c), at constant beam thickness, for a given impact velocity. The length divided by thickness ratio (L/h) of the ice beam is beside the first few experimental points that do not follow the trend of high nondimensional force at low L/L_c ratios.

magnitude. The numerical data also follow this trend where they initially increase relatively quickly at low L/L_c ratios, then appear to asymptotically approach a constant force.

The above comparison suggests that the shortest beams are behaving differently than the longer beams during impact. The data show a more steeply rising nondimensional force for the short beams, which then drops off with increasing L/L_c ratios. This difference is a function of the beam length/thickness ratio (L/h), which determines how the beam reacts during impact. A very small length/thickness ratio would mean that, in profile, the beam would approach a square shape, which would be unstable and easy to roll over at impact. The shortest ice beams would then roll vertically over their upstream bottom corner as they are shoved backwards into the fluid behind the beam during the impact. This behavior would not be as

likely in the numerical simulation, because there is no friction between the bridge face and ice, and therefore no mechanism to push the beam backwards. Furthermore, there is also no "fluid" to hold the upstream bottom corner when the beam is pushed backwards. In the numerical model, these short beams might behave like a rigid body during impact, which would explain the relatively higher peak force in the shortest beams, vs. the impacts against longer or thinner beams where some of the energy went into flexing the ice. This would be similar to the energy required to compress a spring. This scenario would not be as likely in the short, thin ice beams, since the L/h ratio of a short, thin beam is not as large as that of the thick, short beams and thus not as prone to rolling during impact.

The trends in the numerical data support the argument that as the L/L_c ratio of a beam becomes

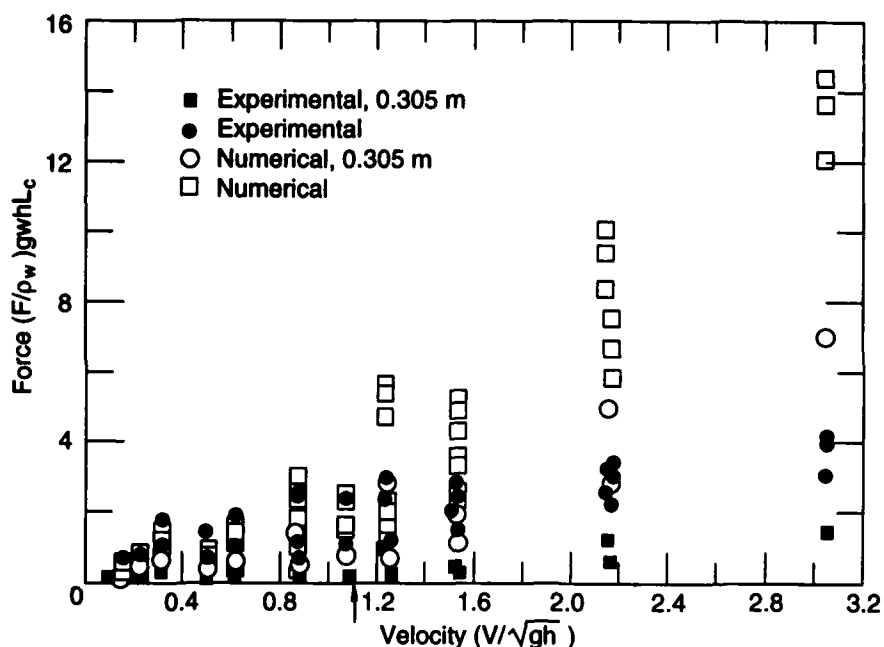


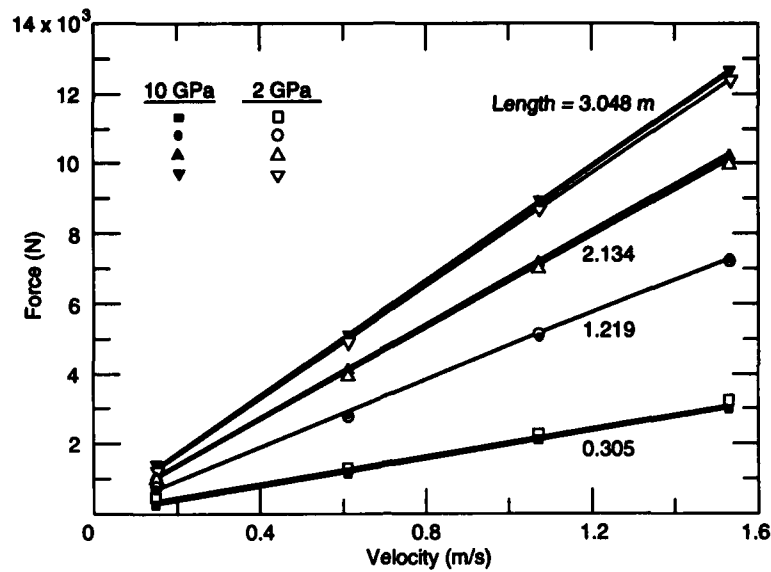
Figure 21. Nondimensional experimental and numerical force vs. nondimensional velocity. The arrow at approximately 1.1 on the velocity scale indicates where the majority of the experimental beams started to be visibly damaged at impact.

larger the force will approach a constant value. The impact velocity will affect the magnitude of this value. The experimental data also tend to approach a constant value with increasing L/L_c ratios, but it is lower overall than what the numerical data suggest. This could be because as the velocity increases, the experimental beams are being damaged, and thus cannot sustain as high an impulsive force as the numerical, purely elastic beam. This is illustrated in Figure 21, which plots nondimensional force vs. velocity, for both the numerical and experimental data. In the figure, the points representing the 0.305-m beams are separate from the other data. The upward pointing arrow on the velocity axis indicates the lowest velocity at which the majority of the experimental beams became damaged. In the figure, the numerical and experimental data start to diverge close to the point where the experimental beams start to break. As the velocity increases the discrepancy becomes greater, while at the lower velocities, the numerical and experimental data compare well.

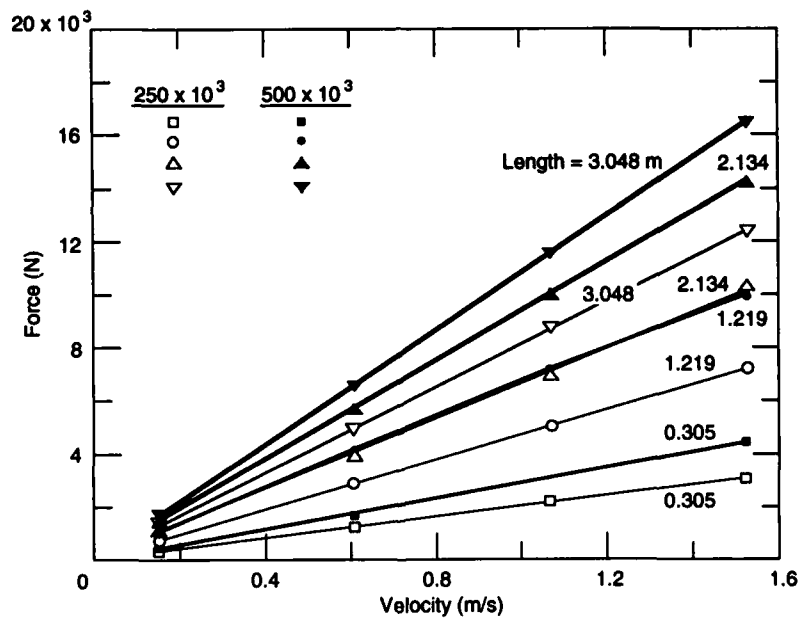
In Figure 21 the nondimensional forces from the experimental 0.305-m beams are below the rest of the experimental data, and the forces from the numerical 0.305-m beams are also below the other numerical data. This trend from the 0.305-m long

beams is evident at nearly every impact velocity and again supports the suggestion that the 0.305-m beams are behaving differently than the other beams. The other differences between the numerical and experimental data for beams of all lengths could be explained by the fact that the experimental beams are breaking while the numerical beams are modeled as perfectly elastic bodies with infinite breaking strength.

Numerical experiments were performed to investigate the effect of changing material properties between the bridge model and ice beam. Figure 22a shows the minimal effect that the change in ice elastic modulus had upon impact force for the 152-mm-thick ice. A much greater effect can be seen in Figure 22b where the effect of changing the structure stiffness is illustrated. At the time of the experimental study, modeling the structure as a rigid body was thought to be acceptable, and that this approximation would give reasonable, if not somewhat high, impact values. Figure 22b, however, illustrates the importance of knowing the structure stiffness during ice impact events. It is evident that a change in structure stiffness would greatly affect the impact force values and an assumption that the structure is rigid could give unacceptable predictions.



a. Plot showing the effect of changing the ice elastic modulus from 2.0 to 10.0 GPa.



b. Plot showing the effect of changing the structure stiffness, from 250×10^3 to 500×10^3 N/m.

Figure 22. Plots of force vs. velocity, at constant beam lengths, from the numerical simulation. These compare the effect, on impact force, of changing the ice elastic modulus vs. changing the structure stiffness.

PROTOTYPE FORCES

Some of the prototype force values that were determined from this study are disturbing in that they seem to be extremely high. However, it should be remembered that the model ice beam sizes

represent a range of prototype sizes from 1.4 m to 79 m. These beams were propelled at a top prototype speed of 3.4 m/s. The larger beams represent a substantial momentum change and thus high forces at the highest velocity tested.

To check the findings, a comparison of the

results of this study with those obtained in the field would be necessary. For the field data to be useful to us, the data needed to include stream velocities, peak impact forces, impact times and the size of the beam that produced the force. Some studies of ice booms that were investigated recorded the first two pieces of information (Perham 1977, 1978, 1983) but not the impact times nor the size of the ice floes creating the force. Some of the peak forces recorded by Perham (1977) were in the 150- to 730-kN range.

However, it is difficult to compare the ice boom force measurements with the impact data. The measured peak force from any impact is dependent upon the duration of the impulse. An ice boom can absorb energy through deflection of the boom and therefore may show a much lower peak force for any given impulse value. The peak force in the modeled situation would probably be higher for any similar floe that strikes an ice boom, since the bridge model is more rigid than a boom. Furthermore, many of these ice boom forces tended to be caused by wind and water drag on large ice sheets as opposed to discrete floes striking the booms.

A report on ice force measurements at a bridge pier (Sodhi and Gagnon 1989, Sodhi et al. 1983), however, gives force measurements attributed to relatively discrete ice floes impacting an instrumented, vertical sided, bridge pier. By direct observation, the river velocity was estimated to be 1.2 to 1.5 m/s, with some of the larger floes that were observed during impact estimated to be 19 to 25 m² large. The forces recorded were predominantly in the 25- to 90-kN range with many above 100 kN. The lower forces presumably came from the smaller brash ice pieces striking the pier. Several impacts were from approximately 130 to 200 kN. The highest actual force recorded was 310 kN.

Our study had three model beam sizes that were close to this prototype range: 17.8, 21.7 and 25.5 m². Our modeled prototype velocity closest to the above velocity range is 1.4 m/s. Our modeled prototype forces for these data range from 137 to 306 kN, which gives good agreement with the larger floe forces measured on vertical, rigid bridge piers. The prototype forces for all of the data are listed in Appendix B.

CONCLUSIONS

A floating beam was subjected to vertical impulsive loads and the resultant beam displace-

ments were measured. The displacements measured in the experiments were modeled using a finite element analysis that designated the ice as a linear elastic material. The dynamic effect of the fluid foundation was calculated in a separate finite element program and added to the numerical beam in the same manner as an added mass matrix. Good agreement between the numerical and experimental results confirmed the validity of the elastic designation and the fluid added mass.

A series of experiments were performed to assess the impact force generated by freshwater ice beams of four different lengths and thicknesses at four velocities. The impact forces from the experiments were numerically modeled using finite element analysis, with an elastic material designation for the ice and the fluid-added mass developed earlier. The conclusions from the work are:

1. The finite element method used in modeling ice/structure impacts allows one to easily model complex geometries, varying impact velocities and different material properties. In the model, the ice is characterized as an elastic body, with a nonlinear foundation modulus to account for the static fluid forces, and a fluid influence coefficient matrix to account for the hydrodynamic fluid forces. The impact forces obtained from the model generally compare well with the experimental data for the thickest ice beams and at the lower velocities for the other thicknesses. The largest discrepancies appear in the forces associated with the very short (0.305-m long) beams. There are also differences evident when the ice fails, which are not accounted for in our model.
2. A failure criteria needs to be developed for the numerical model to properly predict the impact force when the ice beams break.
3. The impact forces caused by the short beams are not modeled well in our present numerical model. As discussed in this report, the inclusion of fluid drag against the bottom and upstream face of the ice beams along with the addition of friction at the bridge/ice interface could correct the short beam's vertical rotation after impact and possibly bring the numerical predictions closer to the experimental results.
4. Ice beam impact forces appear to approach a constant value with increasing beam length for a given impact velocity. This is thought to be a result of the energy absorbed in the flexing of the beam under an impact load, and is described by using the ice's characteristic length. The experimental results appear to agree with the numerical data up until the ice is damaged. The thinnest ice beams

exhibit the same relative trends as the numerical data at all velocities. It should be possible to arrive at a theoretical maximum force, at a given velocity, for long slender beams, based upon a ratio of length divided by characteristic length. In the data, a length/characteristic length ratio of 3 to 5 is where the forces appear to approach a constant value, but more data for longer beams are needed to confirm this upper limit.

5. The structure stiffness is important in determining the impact force in ice/structure interactions. The shape and magnitude of the impulsive force depends heavily upon the reaction of the structure to the impact.

6. The prototype forces calculated from the experiments appear to be in agreement with limited available data of actual force measurements for those cases where the size and velocities of the impacting floes were known.

LITERATURE CITED

- Ashton, G. (1986) *River and Lake Ice Engineering*. Chelsea, Michigan: Book Crafters, Inc.
- Bird R. B., W. Stewart, and E. Lightfoot (1960) *Transport Phenomena*. New York: Wiley.
- Forland, K., J. C. Tatinclaux (1985) Kinetic friction coefficient of ice. CRREL Report 85-6. USA Cold Regions Research and Engineering Laboratory, Hanover, New Hampshire.
- Hetenyi, M. (1946) *Beams on Elastic Foundation*. Ann Arbor: University of Michigan Press.
- Hibbitt, Karlsson and Sorenson, Inc. (1989) ABAQUS users manual. Version 4-8, Hibbitt, Karlsson and Sorenson, Inc., Providence, Rhode Island.
- McGilvary, W. (1989) Analysis of a floating ice sheet undergoing vertical penetration. M. S. Thesis (unpublished), Dartmouth College, Hanover, New Hampshire.
- McGilvary, W., D. Sodhi and J. Lever (1990) Dynamic analysis of a floating ice sheet undergoing vertical indentation. In *Proceedings of the Fourth International Conference on Port and Ocean Engineering Under Arctic Conditions*, vol 2, p. 580-592.
- Perham, R. (1977) St Marys River ice booms, design force estimates and field measurements. CRREL Report 77-4. USA Cold Regions Research and Engineering Laboratory, Hanover, New Hampshire.
- Perham, R. (1978) Performance of the St Marys River ice booms, 1976-1977. CRREL Report 78-24. USA Cold Regions Research and Engineering Laboratory, Hanover, New Hampshire.
- Sharp, J. (1981) *Hydraulic Modelling*. Woburn, Massachusetts: Butterworth Inc.
- Sodhi, D.S., K. Kato and F.D. Haynes (1983) Ice force measurements on a bridge pier in The Ottawaquechee River, Vermont. CRREL Report 83-32. USA Cold Regions Research and Engineering Laboratory, Hanover, New Hampshire.
- Perham, R. (1983) Ice sheet retention structures. CRREL Report 83-30. USA Cold Regions Research and Engineering Laboratory, Hanover, New Hampshire.
- Sodhi, D.S. and J. Gagnon (1989) Ice force measurements on a bridge pier in a small river. In *Proceedings, 10th International Conference on Port and Ocean Engineering Under Arctic Conditions*, Luleå, Sweden, June 12-16, 1989 (K.B.E. Axelsson and L.A. Fransson, Eds), vol. 3, p 1419-27.

APPENDIX A: PRELIMINARY RESULTS AND ANALYSIS

A typical preliminary impact force/time record is shown in Figure A1. The X direction is the top trace, the Y direction is the middle trace and the Z direction is the bottom trace. A downward Z-force trace represents an upward force on the bridge. The impact occurs at about time 1 second and it is evident that the X-force is larger than the Z-force. The face of the bridge is at a 45° angle to the beam which should cause nearly equal X and Z resultant forces on the bridge. In addition, there is also a substantial, oscillating, transverse Y-force. If the beam is lined up perpendicular to the bridge face and strikes it squarely then the amount of force transmitted transverse to the face (Y-direction) will be minimal, probably mostly due to vibration in the model.

Since it is difficult to align a wide beam to strike the bridge squarely, an off-center impact would provide a larger moment arm to rotate the beam about the vertical axis. Figure A2 shows various configurations of beam shapes that were used to determine if the scatter in the data was due to the beams impacting the bridge off-center.

Figure A3 is a graph of X and Z impact forces, plotted against the relative mass of each beam. The largest beam had a relative mass equal to one. The beam mass was changed by changing the width of the beams and by removing material for the different nose shapes.

If the impacts are elastic and no energy is being lost to beam rotation or breakage, then the forces recorded should follow a linear trend against mass, and pass through the origin. In addition, if the experiments are consistent, the scatter of the points at any relative mass should be minimal. It can be seen that the 1.37-m-wide beams with a full width nose had a wide scatter in both the X and Z-forces. The next largest scatter came from the GMC beams (see Fig. A2). These beams had a 0.76-m-wide nose that angled back to the main body of the beam at a 45° angle (Fig. A2). This nose is still relatively wide, which probably contributed to much of the scatter. In

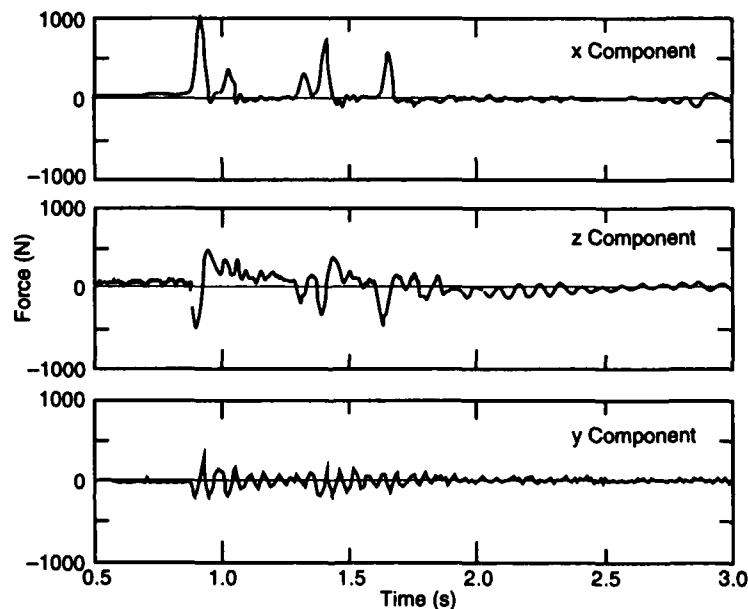
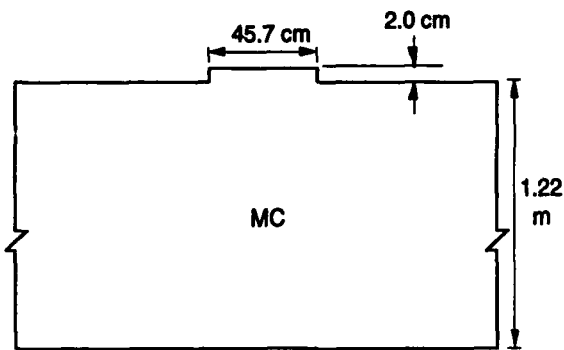
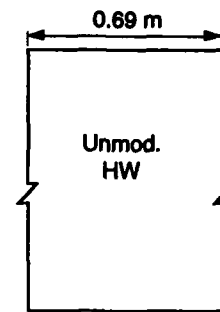


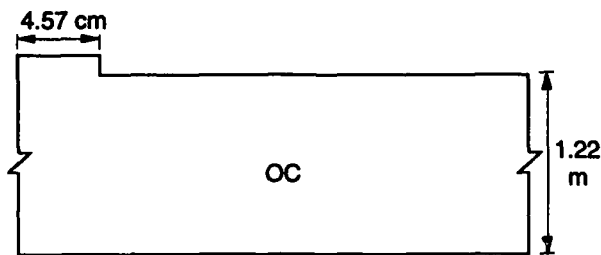
Figure A1. Typical force vs. time record from the preliminary experiments.



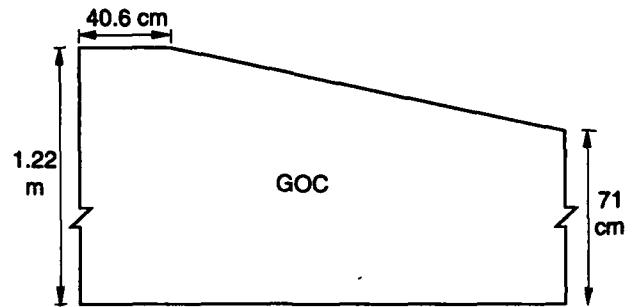
a. Floe MC. This was tried in three widths: 0.76 m, 1.07 m and 1.37 m.



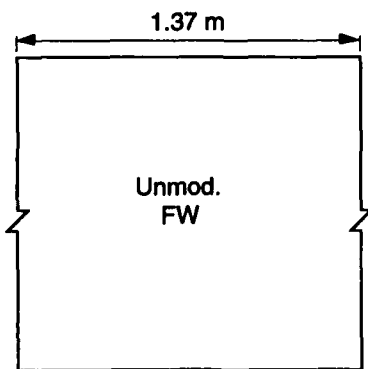
b. Floe HW. This had no protruding nose and was 0.69 m.



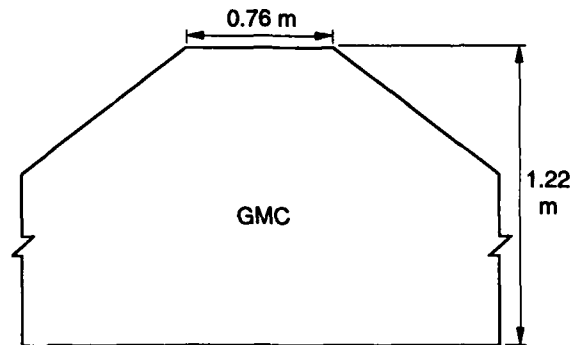
c. Floe OC. 1.37 m wide.



d. Floe GOC. 1.37 m wide.



e. Floe FW. This had no protruding nose and was 1.37 m wide.



f. Floe GMC. 1.37 m wide.

Figure A2. Various floe nose and width combinations, along with their respective labels, used to investigate the high transverse forces found in the preliminary data.

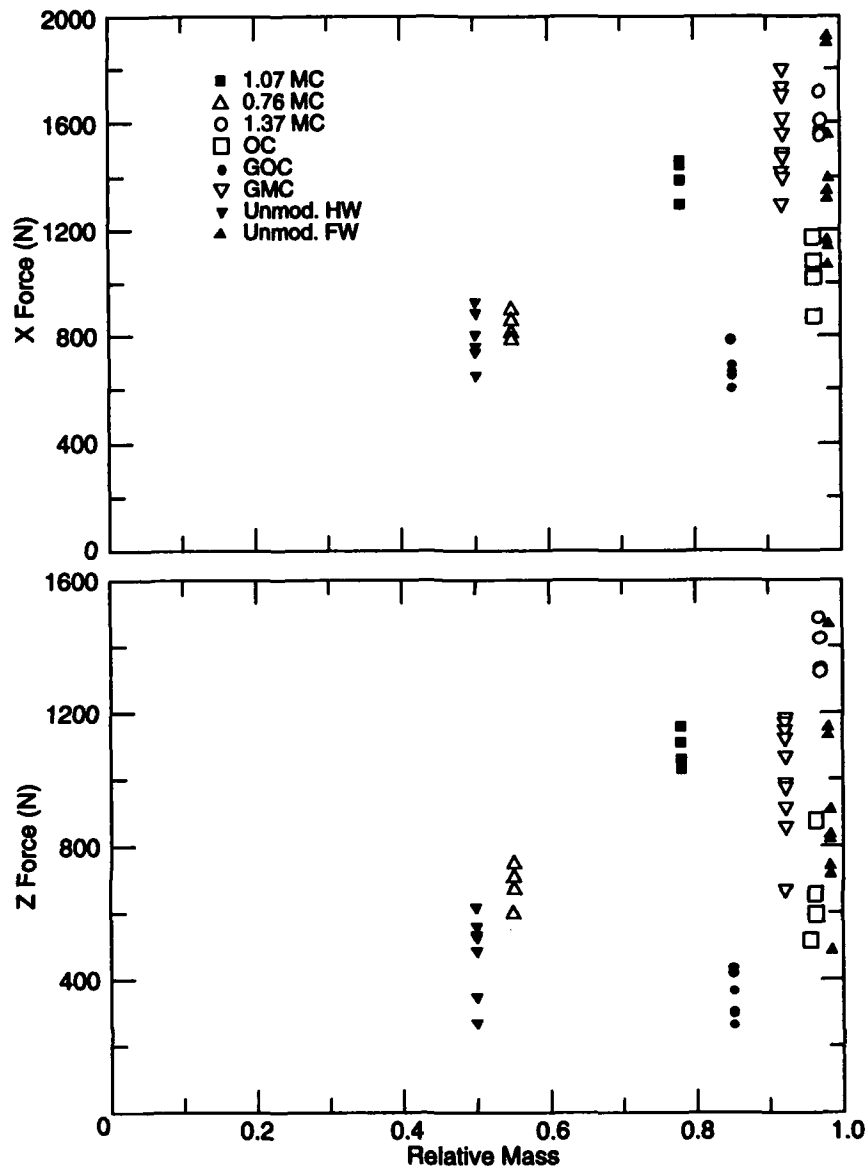


Figure A3. Plot of F_x and F_z vs. beam relative mass.

addition, the Z direction force imparts a bending stress to the beams, causing some to break in tension, at the top surface. The long and relatively narrow beam area behind the nose would present less material to absorb the bending stresses than would a full width beam. This might have contributed to the wider scatter in the forces for these beams. It would be expected, though, that if the beams were breaking prematurely due to the narrower area behind the nose, the average force for these beams would be lower than what it was. It is evident that the forces from the beams with the narrower noses were more consistent.

The beams labeled OC and GOC, in Figure A2, were modified to purposely hit off-center and rotate during impact. Both the X and Z-forces recorded for the GOC beams are well below the others. These beams were the most off-center design used, and it is evident that a lot of energy was expended to rotate the beams. The OC beams did not contain as much mass to one side as the GOC beams did and are more

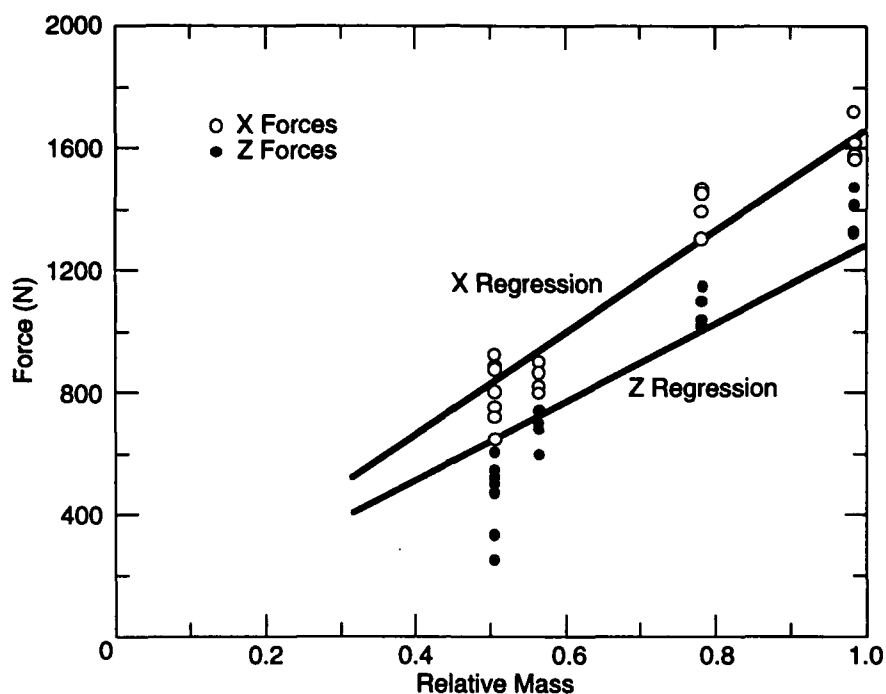


Figure A4. Plot of F_x and F_z vs. beam relative mass, and a best fit linear regression line, through the data, from the origin.

indicative of a full width beam striking slightly out of alignment. These points are below the majority of the data, with the exception of the lower scatter from the full-width beams. This is consistent with the speculation that the lower scatter of the full-width beams is caused by impact with a slightly skewed beam.

The second characteristic looked for in the data was a linear trend through the origin. It can be seen in Figure A3 that beams with FW, OC and GOC shapes fall below any clearly defined linear trend for both the X-force and Z-force data. Furthermore, the GMC beams were excluded because of the scatter and potential breaking problems associated with the longer nose area of these beams.

Figure A4 shows the X and Z-force 1.07 MC, 0.76 MC, 1.37 MC and Unmod HW data that are retained, with the best fit linear regression line through the origin that represents each set. Table A1 lists the model and correlation coefficients for each.

The X-force data are fairly well represented by a linear fit model. A linear fit through the origin does not represent the Z-force data quite as well, but is still reasonable.

Table A2 shows the sample size, average force and standard deviation for the component forces of each type of beam. The magnitude of the standard deviation compared to the average force is also listed and can be used as an indicator of the

Table A1. Slope and correlation coefficients for the regression lines shown in Figure A4.

	Slope	Correlation coefficient
X-force data	1653.85	0.9966
Z-force data	1275.91	0.9856

Table A2. Sample size, average force, standard deviation, and standard deviation divided by average force, of the component forces, for each type of beam used in the preliminary experiments.

Floe description	HW	HW	FW	FW	OC	OC
Force direction	X	Z	X	Z	X	Z
Sample size	26	26	21	20	4	4
Average	1213.6	799.8	1238.5	801.1	1037.5	642.7
Standard deviation	420.4	391.7	470.3	281.0	124.0	154.5
% of avg (S.D./avg)	35%	49%	38%	35%	12%	24%
Floe description	GOC	GOC	1.07 MC	1.07 MC	.76 MC	.76 MC
Force direction	X	Z	X	Z	X	Z
Sample size	6	6	4	4	4	4
Average	675.4	329.2	1396.7	1076.4	844.0	673.9
Standard deviation	58.6	69.5	70.3	57.8	41.9	61.5
% of Avg (S.D./avg)	12%	21%	5%	5%	5%	9%
Floe description	1.37 MC	1.37 MC	GMC	GMC		
Force direction	X	Z	X	Z		
Sample size	4	4	10	10		
Average	1623.5	1382.2	1541.2	987.9		
Standard deviation	64.3	72.7	163.4	162.8		
% of avg (S.D./avg)	4%	5%	11%	17%		

repeatability achieved versus beam type. The modified center beams (MC) gave the best repeatability as is evidenced by the low percentage figures. For this reason the modified center beams were the design used in the experiments.

If the impact strictly follows Newton's 2nd law relationship, then varying the width of the beams, all else being equal, should not affect the impact force, beyond what the corresponding change in mass produces. Figure A5 shows the X and Z-

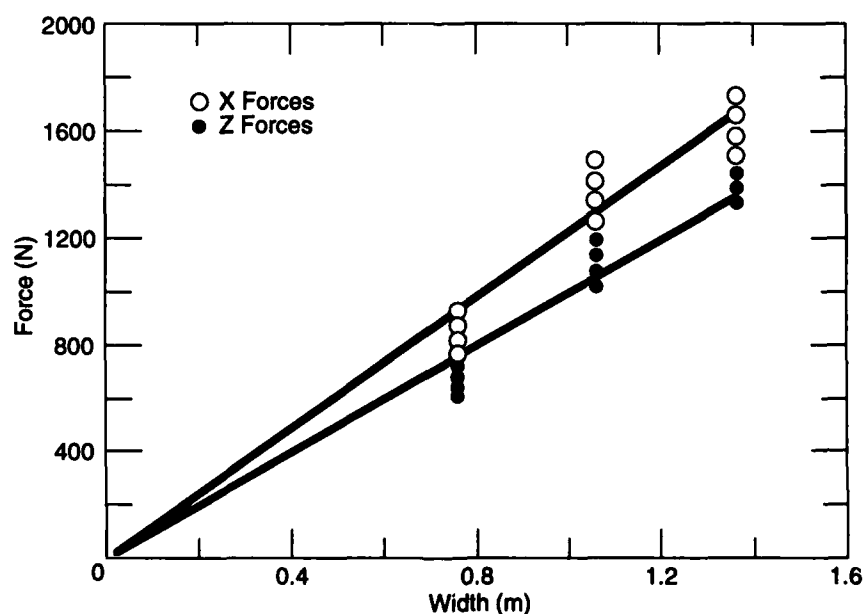


Figure A5. Plot of F_x and F_z vs. ice beam width for the 0.76 MC, 1.07 MC and 1.37 MC beams.

Table A3. Slope and correlation coefficients for the regression lines shown in Figure A5.

	<i>Slope</i>	<i>Correlation coefficient</i>
X-force data	1211.34	0.9952
Z-force data	988.37	0.9954

forces from the 0.76 MC, 1.07 MC and 1.37 MC beams. In these beams only the width was varied while the nose design stayed constant. Although the data did not show a perfect linear force increase with increasing width, it appears quite good as is evidenced by the best fit linear regression line through the origin for each set. Table A3 shows the slopes and correlation coefficients for the data.

In use, the bridge's displacement will change depending upon the load it is carrying. It was not expected that the impact force would be greatly affected by this change but it was prudent to check it. Figure A6 is a graph of impact force vs bridge displacement. The displacement values used modeled the full-scale range, from the no-load displacement up to the maximum expected load value. A higher displacement value means the bridge is deeper into the water. There does not appear to be a significant change in force between the first two displacements. However, at the maximum displacement the X-force appears to drop, while the Z-force rises.

At the low displacement the X-force is greater than the Z-force by an average 138%. It also appears that as the displacement becomes greater the two component forces approach each other in magnitude. With a 45° sloped face one would expect the components to be close to equal disregarding the effect of friction or a dynamic interaction of the model. This characteristic of higher X-forces is noted in the main data and discussed in the report.

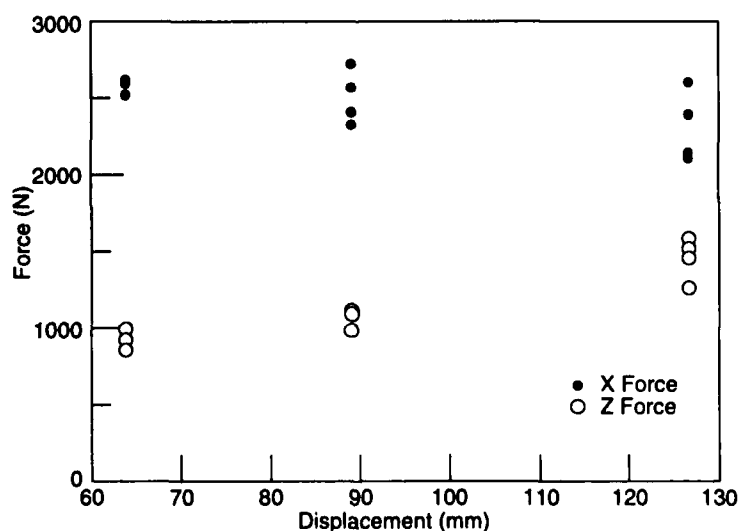


Figure A6. Plot of F_x and F_z vs. model displacement. The beam was 152 mm thick, 1.219 m long and the impact velocity was 0.6096 m/s.

APPENDIX B: TEST DATA.

Damage codes in damage column:

- O – No visible damage
- C – Beam cracked
- B – Beam broke

Model data Model width = 1.372 m						Prototype data Prototype width = 6.86 m				
Floe thick. (m)	Floe length (m)	Velocity (m/s)	X-force (N)	Z-force (N)	Total (N)	Dam.	Floe thick. (m)	Floe length (m)	Vel. (m/s)	Total force (kN)
0.1524	3.048	0.1524	916	765	1193	O	0.762	15.24	0.34	149.2
↓	↓	01524	1517	1148	1902	O	↓	↓	0.34	237.8
●	●	0.1524	1788	1210	2159	O	●	●	0.34	269.9
●	●	01524	1503	1108	1867	O	●	●	0.34	233.4
●	●	0.6096	7024	4826	8522	O	●	●	1.36	1065.3
●	●	0.6096	6548	4662	8067	O	●	●	1.36	1004.7
●	●	0.6096	4938	3398	5994	B	●	●	1.36	749.3
●	●	1.0668	8759	6161	10709	B	●	●	2.39	1338.5
●	●	1.0668	8514	6076	10460	B	●	●	2.39	1307.5
●	●	1.0668	8394	8394	11870	B	●	●	2.39	1483.8
●	●	1.0668	9110	6130	10980	B	●	●	2.39	1372.5
●	●	1.524	10920	7744	13388	B	●	●	3.41	1673.5
●	↑	1.524	11614	8496	14390	B	●	↑	3.41	1798.8
●	3.048	1.524	10916	8065	13572	B	●	15.24	3.41	1696.5
●	2.134	0.1524	747	614	967	O	●	10.67	0.34	120.9
●	↓	01524	907	712	1153	O	●	↓	0.34	144.2
●	●	0.1524	810	810	1145	O	●	●	0.34	143.1
●	●	01524	827	827	1170	O	●	●	0.34	146.3
●	●	0.6096	4395	3087	5371	O	●	●	1.36	671.3
●	●	0.6096	5107	3278	6068	O	●	●	1.36	758.5
●	●	0.6096	5022	3136	5921	O	●	●	1.36	740.1
●	●	0.6096	4493	3149	5487	O	●	●	1.36	685.8
●	↑	1.0668	7638	4688	8962	C	●	↑	2.39	1120.2
●	2.134	1.0668	7228	4466	8497	B	●	10.67	2.39	1062.1
●	1.219	0.1524	418	387	570	O	●	6.10	0.34	71.2
●	↓	0.1524	534	449	698	O	●	↓	0.34	87.2
●	●	0.1524	565	472	736	O	●	●	0.34	92.0
●	●	0.6096	2140	1526	2628	C	●	●	1.36	328.5
●	●	0.6096	2126	1566	2641	O	●	●	1.36	330.1
●	●	0.6096	2393	1463	2805	O	●	●	1.36	350.6
●	●	0.6096	2602	1268	2895	O	●	●	1.36	361.8
●	●	1.0668	4017	2237	4598	C	●	●	2.39	574.7
●	●	1.0668	4350	2220	4884	O	●	●	2.39	610.5
●	●	1.0668	4279	2237	4829	O	●	●	2.39	603.6
●	●	1.0668	4155	2246	4723	O	●	●	2.39	590.4
●	●	1.524	5182	3309	6149	O	●	●	3.41	768.6
↑	↑	1.524	5760	3492	6736	O	↑	↑	3.41	842.0
0.1524	1.219	1.524	5845	2918	6533	C	0.762	6.10	3.41	816.6

Damage codes in damage column:

O – No visible damage

C – Beam cracked

B – Beam broke

Floe thick. (m)	Floe length (m)	Velocity (m/s)	X-force (N)	Z-force (N)	Total (N)	Dam.	Floe thick. (m)	Floe length (m)	Vel. (m/s)	Total force (kN)
0.1524	0.305	0.1524	89	85	123	O	0.762	1.53	0.34	15.3
↓	↓	0.1524	85	85	120	O	↓	↓	0.34	14.9
●	●	0.1524	116	116	164	O	●	●	0.34	20.4
●	●	0.1524	102	120	158	O	●	●	0.34	19.7
●	●	0.6096	476	334	581	O	●	●	1.36	72.7
●	●	0.6096	480	400	625	O	●	●	1.36	78.2
●	●	0.6096	431	285	517	O	●	●	1.36	64.6
●	●	0.6096	458	280	537	O	●	●	1.36	67.1
●	●	1.0668	916	267	954	O	●	●	2.39	119.3
●	●	1.0668	952	307	1000	O	●	●	2.39	125.0
●	●	1.0668	925	569	1086	O	●	●	2.39	135.8
●	●	1.0668	903	436	1003	O	●	●	2.39	125.3
●	●	1.524	1397	472	1474	O	●	●	3.41	184.3
●	●	1.524	1455	276	1480	O	●	●	3.41	185.1
↑	↑	1.524	1477	440	1541	O	↑	↑	3.41	192.6
0.1524	0.305	1.524	1708	445	1765	O	0.762	1.53	3.41	220.6
0.1016	3.048	0.1524	796	805	1132	O	0.508	15.24	0.34	141.5
↓	↓	0.1524	801	850	1167	O	↓	↓	0.34	145.9
●	●	0.1524	894	930	1290	O	●	●	0.34	161.2
●	●	0.1524	921	952	1324	O	●	●	0.34	165.5
●	●	0.6096	4097	3545	5418	B	●	●	1.36	677.2
●	●	0.6096	3954	3501	5281	B	●	●	1.36	660.2
●	●	0.6096	2731	2571	3751	B	●	●	1.36	468.9
●	●	0.6096	3456	2958	4549	B	●	●	1.36	568.7
●	●	1.0668	4849	4039	6310	B	●	●	2.39	788.8
●	●	1.0668	4012	3229	5150	B	●	●	2.39	643.8
●	●	1.0668	4951	4293	6553	B	●	●	2.39	819.1
●	●	1.0668	4791	3750	6084	B	●	●	2.39	760.5
●	●	1.524	5983	4755	7642	B	●	●	3.41	955.3
●	●	1.524	5053	3901	6384	B	●	●	3.41	798.0
●	↑	1.524	5218	4199	6698	B	●	↑	3.41	837.2
●	3.048	1.524	5191	4035	6575	B	●	15.24	3.41	821.8
●	2.134	0.1524	689	716	994	O	●	10.67	0.34	124.3
●	↓	0.1524	783	792	1113	O	●	↓	0.34	139.2
●	●	0.1524	676	689	966	O	●	●	0.34	120.7
●	●	0.1524	774	752	1079	O	●	●	0.34	134.9
●	●	0.6096	3332	2811	4359	O	●	●	1.36	544.9
↑	↑	0.6096	3127	2736	4155	O	↑	↑	1.36	519.4
0.1016	2.134	0.6096	—	—	—	B	0.508	10.67	1.36	—

Damage codes in damage column:

O – No visible damage

C – Beam cracked

B – Beam broke

Floe thick. (m)	Floe length (m)	Velocity (m/s)	X-force (N)	Z-force (N)	Total (N)	Dam.	Floe thick. (m)	Floe length (m)	Vel. (m/s)	Total force (kN)
0.1016	2.134	0.6096	2709	2460	3659	B	0.508	10.67	1.36	457.4
↓	↓	1.0668	3470	2731	4416	B	↓	↓	2.39	552.0
●	●	1.0668	4052	3265	5204	B	●	●	2.39	650.5
●	●	1.0668	3763	3043	4839	B	●	●	2.39	604.9
●	●	1.0668	3705	3078	4817	B	●	●	2.39	602.1
●	●	1.524	4697	3963	6146	B	●	●	3.41	768.2
●	●	1.524	4639	3301	5694	B	●	●	3.41	711.7
●	↑	1.524	4897	3594	6075	B	●	↑	3.41	759.3
●	2.134	1.524	5347	4350	6893	B	●	10.67	3.41	861.6
●	1.219	0.1524	423	414	591	O	●	6.10	0.34	73.9
●	↓	0.1524	378	374	532	O	●	↓	0.34	66.4
●	●	0.1524	418	418	591	O	●	●	0.34	73.9
●	●	0.1524	405	387	560	O	●	●	0.34	70.0
●	●	0.6096	1864	1406	2334	O	●	●	1.36	291.8
●	●	0.6096	1850	1397	2318	O	●	●	1.36	289.8
●	●	0.6096	—	—	—	O	●	●	1.36	—
●	●	0.6096	1962	1459	2445	O	●	●	1.36	305.6
●	●	1.0668	2869	2184	3606	B	●	●	2.39	450.7
●	●	1.0668	2553	2246	3401	B	●	●	2.39	425.1
●	●	1.0668	2798	1971	3422	B	●	●	2.39	427.8
●	●	1.0668	2829	2202	3585	B	●	●	2.39	448.1
●	●	1.524	3349	2589	4233	B	●	●	3.41	529.2
●	●	1.524	3585	2762	4526	B	●	●	3.41	565.7
●	↑	1.524	3536	2785	4501	B	●	↑	3.41	562.6
●	1.219	1.524	3296	2620	4211	B	●	6.10	3.41	526.3
●	0.305	0.1524	80	80	113	O	●	1.53	0.34	14.2
●	↓	0.1524	89	93	129	O	●	↓	0.34	16.1
●	●	0.1524	76	85	113	O	●	●	0.34	14.2
●	●	0.1524	85	18	86	O	●	●	0.34	10.8
●	●	0.6096	236	187	301	O	●	●	1.36	37.6
●	●	0.6096	294	240	379	C	●	●	1.36	47.4
●	●	0.6096	209	196	286	O	●	●	1.36	35.8
●	●	0.6096	111	156	191	O	●	●	1.36	23.9
●	●	1.0668	467	374	598	B	●	●	2.39	74.8
●	●	1.0668	378	325	498	B	●	●	2.39	62.3
●	●	1.0668	374	325	495	O	●	●	2.39	61.9
●	●	1.0668	298	236	380	O	●	●	2.39	47.5
●	●	1.524	547	383	668	B	●	●	3.41	83.5
↑	↑	1.524	618	414	744	B	↑	↑	3.41	93.0
0.1016	0.305	1.524	565	387	685	B	0.508	1.53	3.41	85.6

Damage codes in damage column:

O – No visible damage

C – Beam cracked

B – Beam broke

Floe thick. (m)	Floe length (m)	Velocity (m/s)	X-force (N)	Z-force (N)	Total (N)	Dam.	Floe thick. (m)	Floe length (m)	Vel. (m/s)	Total force (kN)
0.1016	0.305	1.524	520	391	651	B	0.508	1.53	3.41	81.4
0.0508	3.048	0.1524	396	396	560	O	0.254	15.24	0.34	70.0
↓	↓	0.1524	423	440	610	O	↓	↓	0.34	76.3
●	●	0.1524	454	485	664	O	●	●	0.34	83.0
●	●	0.1524	480	498	692	O	●	●	0.34	86.5
●	●	0.6096	961	836	1274	B	●	●	1.36	159.2
●	●	0.6096	1232	983	1576	C	●	●	1.36	197.0
●	●	0.6096	1237	1076	1640	B	●	●	1.36	204.9
●	●	0.6096	1766	1535	2340	C	●	●	1.36	292.4
●	●	1.0668	1828	1201	2187	B	●	●	2.39	273.4
●	●	1.0668	1628	1085	1957	B	●	●	2.39	244.6
●	●	1.0668	1681	930	1921	B	●	●	2.39	240.2
●	●	1.0668	2100	1655	2673	B	●	●	2.39	334.2
●	●	1.524	2469	1775	3041	B	●	●	3.41	380.1
●	●	1.524	2220	1139	2495	B	●	●	3.41	311.8
●	↑	1.524	2447	1552	2897	B	●	↑	3.41	362.2
●	3.048	1.524	2122	1041	2363	B	●	15.24	3.41	295.4
●	2.134	0.1524	351	365	506	B/C	●	10.67	0.34	63.3
●	↓	0.1524	360	396	535	B/C	●	↓	0.34	66.9
●	●	0.1524	387	414	566	B/C	●	●	0.34	70.8
●	●	0.1524	360	387	529	B/C	●	●	0.34	66.1
●	●	0.6096	1250	1072	1647	B	●	●	1.36	205.8
●	●	0.6096	1357	1174	1794	B	●	●	1.36	224.3
●	●	0.6096	890	645	1099	B	●	●	1.36	137.4
●	●	0.6096	1503	1228	1941	B	●	●	1.36	242.6
●	●	1.0668	1757	1437	2270	B	●	●	2.39	283.7
●	●	1.0668	1272	872	1542	B	●	●	2.39	192.8
●	●	1.0668	1606	916	1849	B	●	●	2.39	231.1
●	●	1.0668	1650	1263	2078	B	●	●	2.39	259.8
●	●	1.524	2135	1486	2601	B/C	●	●	3.41	325.1
●	●	1.524	2108	1174	2413	B/C	●	●	3.41	301.7
●	↑	1.524	2019	1259	2380	B/C	●	↑	3.41	297.5
●	2.134	1.524	1704	1014	1983	B/C	●	10.67	3.41	247.8
●	1.219	0.1524	218	227	315	C	●	6.10	0.34	39.3
●	↓	0.1524	173	196	262	O	●	↓	0.34	32.7
●	●	0.1524	231	271	357	O	●	●	0.34	44.6
●	●	0.1524	245	271	365	O	●	●	0.34	45.7
●	●	0.6096	983	970	1381	C	●	●	1.36	172.6
↑	↑	0.6096	632	480	794	B	↑	↑	1.36	99.2
0.0508	1.219	0.6096	1117	979	1485	B	0.254	6.10	1.36	185.6

Damage codes in damage column:

O - No visible damage

C - Beam cracked

B - Beam broke

Floe thick. (m)	Floe length (m)	Velocity (m/s)	X-force (N)	Z-force (N)	Total (N)	Dam.	Floe thick. (m)	Floe length (m)	Vel. (m/s)	Total force (kN)
0.0508	1.219	0.6096	1072	921	1413	B	0.254	6.10	1.36	176.6
↓	↓	1.0668	1174	894	1476	B	↓	↓	2.39	184.5
●	●	1.0668	1246	872	1520	B	●	●	2.39	190.0
●	●	1.0668	1379	912	1653	B	●	●	2.39	206.6
●	●	1.0668	1334	988	1660	B	●	●	2.39	207.5
●	●	1.524	1615	1023	1912	B	●	●	3.41	238.9
●	●	1.524	1481	796	1682	B	●	●	3.41	210.2
●	↑	1.524	1668	930	1910	B	●	↑	3.41	238.7
●	1.219	1.524	1584	934	1839	B	●	6.10	3.41	229.8
●	0.305	0.1524	31	36	47	O	●	1.53	0.34	5.9
●	↓	0.1524	40	36	54	O	●	↓	0.34	6.7
●	●	0.1524	49	36	61	O	●	●	0.34	7.6
●	●	0.1524	40	36	54	O	●	●	0.34	6.7
●	●	0.6096	147	165	221	O	●	●	1.36	27.6
●	●	0.6096	173	142	224	O	●	●	1.36	28.1
●	●	0.6096	142	165	218	O	●	●	1.36	27.2
●	●	0.6096	178	120	215	O	●	●	1.36	26.8
●	●	1.0668	218	222	311	B	●	●	2.39	38.9
●	●	1.0668	222	191	293	B	●	●	2.39	36.7
●	●	1.0668	231	218	318	B	●	●	2.39	39.7
●	●	1.0668	231	227	324	B	●	●	2.39	40.5
●	●	1.524	302	178	351	B	●	●	3.41	43.9
●	●	1.524	400	307	504	B	●	●	3.41	63.1
↑	↑	1.524	378	271	465	B	↑	↑	3.41	58.2
0.0508	0.305	1.524	338	347	484	B	0.254	1.53	3.41	60.6
0.0254	3.048	0.1524	267	285	390	O	0.127	15.24	0.34	48.8
↓	↓	0.1524	316	298	434	O	↓	↓	0.34	54.3
●	●	0.1524	227	249	337	O	●	●	0.34	42.1
●	●	0.1524	320	325	456	O	●	●	0.34	57.0
●	●	0.6096	347	365	503	B	●	●	1.36	62.9
●	●	0.6096	—	—	—	B	●	●	1.36	—
●	●	0.6096	356	343	494	B	●	●	1.36	61.7
●	●	0.6096	480	516	705	B	●	●	1.36	88.1
●	●	1.0668	707	503	868	B	●	●	2.39	108.5
●	●	1.0668	547	454	711	B	●	●	2.39	88.8
●	●	1.0668	654	467	804	B	●	●	2.39	100.4
●	●	1.0668	569	414	704	B	●	●	2.39	88.0
●	●	1.524	885	494	1014	B	●	●	3.41	126.7
↑	↑	1.524	649	436	782	B	↑	↑	3.41	97.8
0.0254	3.048	1.524	943	627	1133	B	0.127	15.24	3.41	141.6

Damage codes in damage column:

O – No visible damage

C – Beam cracked

B – Beam broke

Floe thick. (m)	Floe length (m)	Velocity (m/s)	X-force (N)	Z-force (N)	Total (N)	Dam.	Floe thick. (m)	Floe length (m)	Vel. (m/s)	Total force (kN)
0.0254	3.048	1.524	792	427	900	B	0.127	15.24	3.41	112.4
0.0254	2.134	0.1524	258	258	365	O	0.127	10.67	0.34	45.6
↓	↓	0.1524	258	240	353	O	↓	↓	0.34	44.1
●	●	0.1524	231	258	347	O	●	●	0.34	43.3
●	●	0.1524	254	240	349	O	●	●	0.34	43.7
●	●	0.6096	632	694	938	B	●	●	1.36	117.3
●	●	0.6096	—	—	—	C	●	●	1.36	—
●	●	0.6096	431	418	601	B	●	●	1.36	75.1
●	●	0.6096	338	360	494	C	●	●	1.36	61.8
●	●	1.0668	587	601	840	B	●	●	2.39	105.0
●	●	1.0668	383	276	472	B	●	●	2.39	58.9
●	●	1.0668	454	320	555	B	●	●	2.39	69.4
●	●	1.0668	427	347	550	B	●	●	2.39	68.8
●	●	1.524	881	512	1019	B	●	●	3.41	127.3
●	●	1.524	743	543	920	B	●	●	3.41	115.0
●	↑	1.524	676	525	856	B	●	↑	3.41	107.0
●	2.134	1.524	810	725	1087	B	●	10.67	3.41	135.8
●	1.219	0.1524	187	200	274	O	●	6.10	0.34	34.2
●	↓	0.1524	173	178	249	O	●	↓	0.34	31.1
●	●	0.1524	156	169	230	O	●	●	0.34	28.7
●	●	0.1524	182	214	281	O	●	●	0.34	35.1
●	●	0.6096	449	534	698	B	●	●	1.36	87.2
●	●	0.6096	365	343	500	B	●	●	1.36	62.5
●	●	0.6096	369	396	541	B	●	●	1.36	67.7
●	●	0.6096	338	302	454	B	●	●	1.36	56.7
●	●	1.0668	525	472	706	B	●	●	2.39	88.2
●	●	1.0668	596	485	768	B	●	●	2.39	96.0
●	●	1.0668	516	387	645	B	●	●	2.39	80.6
●	●	1.0668	436	338	552	B	●	●	2.39	69.0
●	●	1.524	636	387	745	B	●	●	3.41	93.1
●	●	1.524	636	351	727	B	●	●	3.41	90.8
●	↑	1.524	498	391	634	B	●	↑	3.41	79.2
●	1.219	1.524	667	347	752	B	●	6.10	3.41	94.0
●	0.305	0.1524	31	49	58	O	●	1.53	0.34	7.3
●	↓	0.1524	49	62	79	O	●	↓	0.34	9.9
●	●	0.1524	40	62	74	O	●	●	0.34	9.3
●	●	0.1524	40	49	63	O	●	●	0.34	7.9
●	●	0.6096	125	160	203	O	●	●	1.36	25.4
↑	↑	0.6096	142	151	208	O	↑	↑	1.36	26.0
0.0254	0.305	0.6096	125	129	179	O	0.127	1.53	1.36	22.4

Damage codes in damage column:

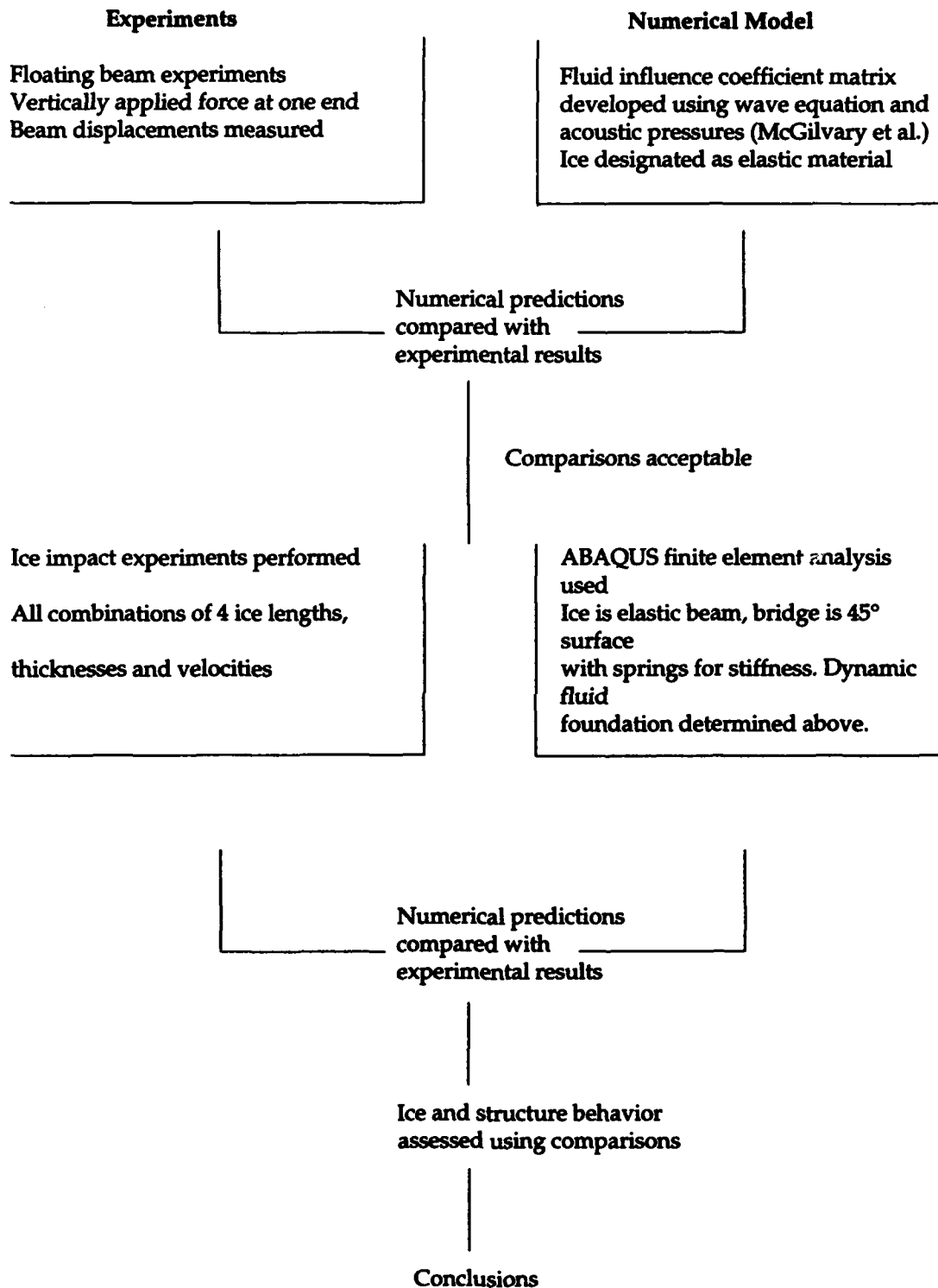
O – No visible damage

C – Beam cracked

B – Beam broke

Floe thick. (m)	Floe length (m)	Velocity (m/s)	X-force (N)	Z-force (N)	Total (N)	Dam.	Floe thick. (m)	Floe length (m)	Vel. (m/s)	Total force (kN)
0.0254	0.305	0.6096	125	129	179	B	0.127	1.53	1.36	22.4
↓	↓	1.0668	182	187	261	B	↓	↓	2.39	32.6
●	●	1.0668	191	173	258	B	●	●	2.39	32.3
●	●	1.0668	214	276	349	B	●	●	2.39	43.6
●	●	1.0668	187	200	274	B	●	●	2.39	34.2
●	●	1.524	245	182	305	B	●	●	3.41	38.1
●	●	1.524	258	173	311	B	●	●	3.41	38.9
↑	↑	1.524	267	205	336	B	↑	↑	3.41	42.0
0.0254	0.305	1.524	249	200	320	B	0.127	1.53	3.41	39.9

APPENDIX C: PROCEDURE FLOW CHART



REPORT DOCUMENTATION PAGE

Form Approved
OMB No. 0704-0188

Public reporting burden for this collection of information is estimated to average 1 hour per response, including the time for reviewing instructions, searching existing data sources, gathering and maintaining the data needed, and completing and reviewing the collection of information. Send comments regarding this burden estimate or any other aspect of this collection of information, including suggestion for reducing this burden, to Washington Headquarters Services, Directorate for Information Operations and Reports, 1215 Jefferson Davis Highway, Suite 1204, Arlington, VA 22202-4302, and to the Office of Management and Budget, Paperwork Reduction Project (0704-0188), Washington, DC 20503.

1. AGENCY USE ONLY (Leave blank)		2. REPORT DATE March 1994		3. REPORT TYPE AND DATES COVERED	
4. TITLE AND SUBTITLE Experimental and Numerical Analysis of Floating Ice Beam Impact Against a Sloped Structure				5. FUNDING NUMBERS	
6. AUTHORS Barry A. Coutermarsh					
7. PERFORMING ORGANIZATION NAME(S) AND ADDRESS(ES) U.S. Army Cold Regions Research and Engineering Laboratory 72 Lyme Road Hanover, N.H. 03755-1290				8. PERFORMING ORGANIZATION REPORT NUMBER CRREL Report 94-2	
9. SPONSORING/MONITORING AGENCY NAME(S) AND ADDRESS(ES) U.S. Army Cold Regions Research and Engineering Laboratory 72 Lyme Road Hanover, N.H. 03755-1290				10. SPONSORING/MONITORING AGENCY REPORT NUMBER	
11. SUPPLEMENTARY NOTES					
12a. DISTRIBUTION/AVAILABILITY STATEMENT Approved for public release; distribution is unlimited. Available from NTIS, Springfield, Virginia 22161.				12b. DISTRIBUTION CODE	
13. ABSTRACT (Maximum 200 words) Floating ice impact forces are of concern where structures are built in ice-susceptible waters. Bridge piers, ice control structures or icebreakers are a few examples where the ability to predict the expected ice impact force would be of great help in the design process. Experiments were performed to determine the response of a floating ice beam to a vertically applied force. The data were used to calibrate a numerical finite element model of the floating ice. The ice was characterized as a linear elastic material in the numerical analysis, and the calibration data were used to assess this assumption as well as to develop a fluid influence coefficient matrix to simulate the dynamic influence of the fluid beneath the ice beam. Finally, a scale model study was performed to determine actual impact forces generated by a floating ice beam against a 45° sloped structure. The numerical model developed was then compared to the actual data. The numerical model does well at predicting impact forces for all the beams at low velocity and the force from the thicker ice beams at all velocities. Both the numerical and experimental forces show the same trends and appear to level off and approach a constant value with increasing beam length. The discrepancies between numerical predictions and experimental results are thought to be caused by damage in the experimental ice beams which is not accounted for in the numerical model.					
14. SUBJECT TERMS Freshwater ice Impact forces Ribbon bridge Sloped structures				15. NUMBER OF PAGES 45	
				16. PRICE CODE	
17. SECURITY CLASSIFICATION OF REPORT UNCLASSIFIED	18. SECURITY CLASSIFICATION OF THIS PAGE UNCLASSIFIED	19. SECURITY CLASSIFICATION OF ABSTRACT UNCLASSIFIED	20. LIMITATION OF ABSTRACT UL		